Palaeogeography, Palaeoclimatology, Palaeoecology

A palaeogeographic context for Neoproterozoic glaciation

Paul F. Hoffman[a,b,c,*] and Zheng-Xiang Li[d]

[a] *Department of Earth and Planetary Sciences, Harvard University, Cambridge, Massachusetts 02138, USA*

[b] *Geology & Geophysics, School of Earth and Environmental Sciences, The University of Adelaide, Adelaide, SA 5004, Australia*

[c] *School of Earth and Ocean Sciences, University of Victoria, Victoria, British Columbia V8W 2Y2, Canada*

[d] *Institute for Geoscience Research, Curtin University of Technology, GPO Box U1987, Perth, WA 6845, Australia*

* Corresponding author.
3271 Wicklow St., Victoria, BC, Canada V8X 1E1 (Tel. +1 250 380 0059)
E-mail address: paulfhoffman@yahoo.com (P.F. Hoffman)

Abstract

The distributions of 77 Neoproterozoic glacigenic formations are shown on global palaeogeographic maps for 715 Ma (Sturtian), 635 Ma (Marinoan) and 580 Ma (Ediacaran), constructed on grounds independent of palaeoclimatic indicators. The meridional distribution of Sturtian and Marinoan deposits is biased in favour of low palaeolatitudes, whereas Ediacaran deposits are biased in favour of high palaeolatitudes. All carbonate-hosted glacigenic formations (n=22) fall within 35 degrees of the palaeoequator. Most (6 of 8) examples of periglacial polygonal sand-wedges occur at palaeolatitudes greater than 30 degrees, whereas most (8 of 9) occurrences of large syn-glacial Fe and Fe-Mn deposits lie within 30 degrees of the palaeoequator. Marinoan syn-deglacial cap dolostones (n=24) decline in maximum thickness with palaeolatitude, consistent with poleward ice retreat, normal meridional temperature gradients and a small-obliquity orbit. Meridional (N-S) mean orientations of giant wave ripples in Marinoan cap dolostones from different regions (n=10) and absence of zonal (W-E) orientations are consistent with zonal wind-driven waves and not with hurricanes. In general, the results support the validity of the palaeogeographic reconstructions and the pan-glacial character of Sturtian and Marinoan ice ages.

Keywords: Neoproterozoic; Palaeogeography; Snowball Earth; Banded iron-formation; Cap carbonate; Giant wave ripples.

1. Introduction

The hypothesis that Cryogenian glaciations (750-635 Ma) glaciations were more severe than any subsequent ones—possibly involving dynamic glaciers of global extent—rests heavily (but not exclusively) on palaeomagnetic data (Embleton and Williams, 1986; Kirschvink, 1992; Schmidt and Williams, 1995; Sohl et al., 1999; Evans, 2000, 2003; Trindade and Macouin, 2007). For example, a pair of discrete glacigenic formations found along the margin of Laurentia from California to northwestern Canada were deposited close to the palaeoequator according to robust palaeomagnetic poles from mafic igneous suites precisely dated at 780, 723 and 615 Ma. Yet, there is confusion as well as uncertainty concerning the palaeogeographic context of the glacial intervals. Published general circulation models (GCMs), for instance, employ palaeogeographic models ranging from a polar supercontinent (Hyde et al., 2000; Peltier et al., 2004, 2007) to a band of fragmented low-latitude continents (Goddéris, et al., 2003; Donnadieu et al., 2004a, b). With regard to the geochemical carbon cycle, the first palaeogeography should yield a globally warm climate (Worsley and Kidder, 1991) and the second a cold one (Donnadieu et al., 2004a).

Evans (2000, 2003), Chumakov (2004) and Trindade and Macouin (2007) have synthesized the stratigraphic, geochronologic and palaeomagnetic constraints on Neoproterozoic glaciations, which post-date the breakup of the Rodinia supercontinent. There were three main glacial episodes, commonly referred to in the current literature as Sturtian, Marinoan and Gaskiers (e.g., Halverson, 2006). Sturtian and Marinoan were originally defined as chronostratigraphic terms (Mawson and Sprigg, 1950; see also

Preiss, 1987). Strictly speaking, the Sturtian ends stratigraphically well above the glacigenic Sturt Formation and its correlatives. As originally defined, the Marinoan begins well below the glacigenic Elatina Formation and continues to the end of the Precambrian. However, the internationally recognized Ediacaran and Cryogenian (when formally defined) periods will soon render Sturtian and Marinoan obsolete in their original meaning. Meanwhile, the terms have come to be used almost universally with reference to Cryogenian glacial periods of global or near global extent.

This use has been criticized as amounting to a circular argument: global glaciation both depends upon, and is the justification for, the correlation of glacial deposits. This criticism is based on a misunderstanding. The case for global glaciation rests not on correlation, but on combined sedimentological and palaeomagnetic evidence that Sturtian and Marinoan ice sheets reached sea-level close to the palaeoequator (Kirschvink, 1992; Evans, 2000), including areas where no mountains existed (Hoffman, 2005). This, and the occurrence of ice-proximal deposits conformably within thick marine carbonate successions (Hoffman and Halverson, 2008; Macdonald et al., 2009a) proves that ice sheets flowed into the warmest parts of the surface ocean. If ice sheets existed at sea level in the warmest parts of the world, then higher latitudes and elevations must have been frozen as well. This, not correlation, is the rationale for global glaciation. Correlation follows from the premise; it is not a precondition.

Gaskiers is the name of a mid-Edicaran (582 Ma) glacigenic formation in eastern Canada; it was never a chronostratigraphic term. Its global application is inadviseable because evidence for low-latitude glaciation at this time is weak. In this paper, we refer to the Gaskiers and other Ediacaran glaciation(s) as Ediacaran. We do not deduce that the Ediacaran glaciations were correlative although, for want of geochronological data, we plot them on a single palaeogeographic map.

According to the best current geochronological data, Sturtian glaciation(s) occurred between roughly 726 and 660 Ma (Bowring et al., 2007; Fanning and Link, 2008) and Marinoan between roughly 655 Ma and 635 Ma (Condon et al., 2005; Zhang et al., 2008). There are unconfirmed reports of glaciation(s) between roughly 755 Ma and 726 Ma (Frimmel et al., 1996; Key et al., 2001; Borg et al., 2003; Xu et al., 2009). We refer to these as pre-Sturtian.

Recently, a new set of palaeogeographic models (Li et al., 2008) for the Neoproterozoic eon were generated as part of an international effort by the Tectonics Special Research Centre in Perth, Western Australia, established by the late Christopher McA. Powell. The reconstructions derive from a multi-disciplinary approach, utilizing geological provincial linkages, tectonostratigraphic correlations and the mantle-plume record, in addition to palaeomagnetic constraints (listed in Table 1 of Li et al., 2008 and Table 1 of Pisarevsky et al., 2008, with new data discussed in the next paragraph). Palaeomagnetic constraints are strongest for Australia and Amazonia in the Marinoan, and for Laurentia in the Sturtian and Ediacaran. Palaeogeographic maps representing 5-Myr time-slices were constructed by interpolation between palaeomagnetic and geological control points, including the Early Cambrian formation of Gondwanaland.

Importantly, the glacial record played no role in the reconstructions. In this paper, we plot the respective glacigenic deposits on palaeogeographic model maps for 715 (Sturtian), 635 (Marinoan) and 580 (Ediacaran) Ma (Li et al., 2008). We do this as a means of comparing the three glacial episodes with each other and with other glaciations in Earth history. Further, we use specific aspects of the glacial-associated palaeoclimate record to test the palaeogeographic models themselves.

We use a revised position for East Svalbard, with respect to Laurentia, based on new palaeomagnetic results (Maloof et al., 2006). Otherwise, the model maps are the same as those in Li et al. (2008). The position of North Slope terrane of Arctic Alaska, rotated against the Arctic margin of Laurentia (Li et al., 2008), is challenged by new studies of its Neoproterozoic-Cambrian stratigraphy (Macdonald et al., 2009b). The Euler poles used in constructing the maps can be found in Appendix III of Li et al. (2008) and the Euler pole for rotating East Svalbard to Laurentia is situated at 81°S, 125°E with 68° of rotation (Maloof et al., 2006). For the 580-Ma model, we adopt the high-latitude option for Laurentia, consistent with recent palaeomagnetic results from the 590-Ma Grenville dykes (K. Buchan, unpublished data).

Following Hoffman (2009), we use the term "pan-glacial" for climate states in which continents at all latitudes have ice sheets but the extent of ocean ice-cover is unspecified, "snowball earth" for a pan-glacial state in which the oceans are covered by floating glaciers and "slushball earth" for one in which the oceans are mostly ice-free.

2. Geochronology of Neoproterozoic glaciations

We group Neoproterozoic glacigenic deposits into 77 formations on 22 palaeocontinents (Table 1).

2.1. Geochronology of Ediacaran glaciations

Ediacaran glaciations are recognized on at least 8 palaeocontinents (Table 1, Fig. 1A), but only the Gaskiers Formation on the Avalon Peninsula of eastern Newfoundland, Canada, has been directly dated (Fig. 2). U-Pb zircon geochronology by isotope-dilution thermal-ionization mass spectrometry (ID-TIMS) of subaqueous volcanic tuff horizons below, within and above the glacigenic Gaskiers Formation constrains the onset of glaciation to post-date 583.7±0.5 (all ages cited with 2σ uncertainties) and its termination to pre-date 582.1±0.5 Ma (Bowring et al., 2003; S.A. Bowring, pers. comm. 2006). The maximum allowable duration of the Gaskiers glaciation of 2.6 Myr makes it unlikely to represent a snowball earth because millions of years of atmospheric CO_2 accumulation would be required for its deglaciation (Walker et al., 1981; Caldeira and Kasting, 1992; Pierrehumbert, 2004). Accordingly, we cannot infer that Ediacaran glaciations on other palaeocontinents (Table 1) were synchronous with the Gaskiers glaciation.

2.2. Geochronology of Marinoan (younger Cryogenian) glaciations

Despite their great age, Marinoan glacigenic deposits are the most widespread in Earth history, occurring on at least 15 palaeocontinents (Table 1, Fig. 1B). The Ghaub Formation in Namibia is directly dated by U-Pb (ID-TIMS) at 635.6±0.5 Ma (Hoffmann et al., 2004), the Fiq Formation in Oman by the same method at 640±10 Ma (Bowring et al., 2007) and the Nantuo Formation in South China by 'sensitive high-resolution ion microprobe' (SHRIMP) at 636.3±4.9 Ma (S. Zhang et al., 2008). In South China, zircons from a tuff at the top of the syndeglacial 'cap' dolostone give a U-Pb (ID-TIMS) age of 635.2±0.4 Ma (Condon *et al.,* 2005), constraining the glacial termination, while a U-Pb (SHRIMP) age of 654.5±3.8 Ma (S. Zhang et al., 2008) from a tuff near the top of the Datangpo Formation, which underlies the Nantuo Formation, is interpreted as a maximum bound on the glacial onset (Fig. 3). Accordingly, the maximum duration of the Nantuo glaciation is 23.5 Myr. However, the Nantuo Formation itself appears to have been deposited over a much shorter time interval near the end of the glacial period (Fig. 4). Glaciations on other palaeocontinents (Table 1) are correlated with the Ghaub and Nantuo glaciations based primarily on isotopic and lithological similarities between their respective 'cap' dolostones (Dunn et al., 1971; Kennedy et al., 1998; James et al., 2001; Allen et al., 2005a; Shields, 2005; Hoffman et al., 2007).

2.3. Geochronology of Sturtian (older Cryogenian) glaciations

Sturtian glaciation(s) was almost as widespread as Marinoan, being recognized on at least 14 palaeocontinents (Table 1, Fig. 1C). However, there is considerably more uncertainty regarding the number and duration of glacial episodes (Fig. 5). Syn-glacial U-Pb ages have been reported from three palaeocontinents: 723+16/-10 Ma (SHRIMP) and 711.5±0.3 Ma (TIMS) for the Gubrah Formation in Oman (Brasier et al., 2000; Bowring et al., 2007), 686±4 Ma (SHRIMP) for the Scout Mountain Member of the Pocatello Formation in southern Idaho, USA (Fanning and Link, 2008), 685±7 and 684±4 Ma (SHRIMP) from the Edwardsburg Formation of central Idaho, USA (Lund et al., 2003), and 659.7±5.3 Ma for the Wilyerpa Formation in South Australia (Fanning and Link, 2008). The minimum 56-Myr spread between these ages has understandably caused many to question the existence of a single synchronous glaciation during this interval. However, some of the ages themselves are open to question. Zircons from the Gubrah Formation dated at 723+16/-10 Ma could be detrital in origin (Brasier et al., 2000) and were extracted from the same horizon subsequently dated more precisely at 711.5±0.3 Ma (Bowring et al., 2007). The 686±4 Ma age for the Scout Mountain Member (Fanning and Link, 2008) is from a sample reported earlier as 709±4 Ma (Fanning and Link, 2004) that is not exposed in contact with glacigenic strata. The ages from central Idaho (Lund et al., 2003) come from a tectonized paraconglomerate within a roof pendant of the Idaho Batholith (Cretaceous) and its glacial origin is unproved. The 659.7±5.3 Ma age from South Australia (Fanning and Link, 2008) is from a silt- and sand-dominated unit (Wilyerpa Formation) with rare lonestones that separates glacigenic diamictites of the Sturt Formation from thick transgressive shale of the Tapley Hill Formation. Strictly speaking, it represents a minimum age constraint on the Sturtian glaciation, but would be close to the glacial termination in age if the Tapley Hill transgression is related to glacioeustatic flooding. A Re-Os isochron age of 643±2.4 Ma (Kendall et al., 2006) was obtained from black shale of the Tindelpina Member at the base of the Tapley Hill

Formation and an age of 657.2±5.4 Ma (Kendall et al., 2006) by the same method was determined for the broadly correlative Aralka Formation in the subsurface of central Australia. The age of 659.7±5.3 Ma (Fanning and Link, 2008) for the Sturtian glacial termination leaves little time for the deposition of thick shelfal successions found between the Sturtian and Marinoan glaciations in Australia and elsewhere. In northern Namibia, for example, the Chuos and Ghaub formations (Table 1) are separated by 500-800 m of platformal carbonate strata.

We consider the Gubrah age of 711.5±0.3 Ma (Bowring et al., 2007) to be the the best currently available for Sturtian glaciation, but acknowledge that muliple and/or a very prolonged (≥53 Myr) glaciation cannot be ruled out. We take 726±1 Ma (Bowring et al., 2007) and 659.7±5.3 Ma (Fanning and Link, 2008) as the best maximum and minimum constraints, respectively.

The case for pre-726±1 Ma glaciation rests on the validity and stratigraphic interpretation of a U-Pb (SHRIMP) age of 752±6 Ma (Borg et al., 2003) from the Port Nolloth Group of southwest Namibia, a similar age of 735±5 Ma (Key et al., 2001) from the Katanga Supergroup of Zambia, and a Pb-Pb zircon evaporation age of 741±6 Ma (Frimmel et al., 1996) from the Rosh Pinah Formation of southwest Namibia. The structural geology in both areas is complex and primary stratigraphic relations between glacigenic units and the dated horizons require further study. Recently, U-Pb (SHRIMP) ages of 740±7 and 725±10 Ma (Xu et al., 2009) were obtained from volcanic beds within diamictites of the Bayisi Formation of northwest China. A glacial origin for the Bayisi diamictites remains uncertain (Norin, 1937; Xiao et al., 2004; Xu et al., 2009).

3. Palaeogeography of Neoproterozoic glaciations

In Fig. 6, we plot the locations (stars) of established glacigenic formations (Table 1) on the palaeogeographic model maps for 580, 635 and 715 Ma (Li et al., 2008). The stars are colour-coded according to the dominant sedimentary lithology of the immediate pre-glacial succession: blue for carbonate, green for mixed carbonate-siliciclastic, yellow for siliciclastic, and white for volcanic successions or where there is a major hiatus beneath the glacigenic formation. Stars with heavy black outlines indicate glacigenic formations containing polygonal sand wedges and stars outlined in red connote formations containing synglacial sedimentary iron- or iron-manganese deposits.

The lithologic character of pre-glacial successions provides an independent test of the palaeogeographic reconstructions (Li et al., 2008). Because of the 'reverse' solubility of $CaCO_3$ and $(CaMg)CO_3$ (i.e., degree of saturation decreases with cooling and pressure, and increases with warming), Phanerozoic shallow-water carbonate deposition occurred mainly within 35° of the palaeoequator (Blackett, 1961; Opdyke, 1962; Briden and Irving, 1964; Briden, 1970; Ziegler et al., 1984; Kiessling, 2001), the same as in the Recent (Rodgers, 1957). This was particularly true for non-skeletal carbonates (Opdyke and Wilkinson, 1990); so-called 'cool-water' carbonates depend on the ability of certain skeletal animals, notably bryozoans and certain molluscs and foraminifers, to precipitate carbonate from undersaturated waters. The meridional range of shallow-water carbonates did not vary perceptibly between warm and cool periods of the Phanerozoic (Kiessling, 2001). This is because the distribution of carbonate deposition depends on the relative, not the absolute, temperature, and perhaps also because the flux of alkalinity into the ocean (which ultimately drives carbonate production) was augmented by glacial action during cool periods, when rainfall and therefore weathering rates were somewhat diminished.

The occurrence of Neoproterozoic carbonate-dominated and mixed carbonate-siliciclastic successions at palaeolatitudes <35° (Fig. 6) validates the palaeogeographic reconstructions for 715, 635 and 580 Ma (Li et al., 2008). And it provides additional support for a poleward decrease in palaeotemperatures and therefore a low-obliquity orbital configuration (Evans, 2006). As expected, siliciclastic-dominated sequences occur at all palaeolatitudes (Fig. 6).

3.1. Meridional distribution of glacigenic formations

Evans (2000, 2003) gives histograms of the frequency of occurrence of glacigenic formations over time as a function of palaeomagnetically-constrained palaeolatitude. The histograms are limited by the relatively small number of reliable palaeomagnetic determinations for Proterozoic glacigenic formations. In Fig. 7, we plot histograms of Neoproterozoic glacigenic formations as a function of palaeolatitude based on the palaeogeographic maps (Fig. 6) compiled by Li et al. (2008). Although the maps are subject to numerous uncertainties, the histograms nonetheless reveal striking differences between the Cryogenian and Ediacaran glaciations.

Sturtian and Marinoan glacigenic formations plot disproportionately at middle and low palaeolatitudes (<45°), with maxima at equatorial palaeolatitudes (<15°). None are at palaeolatitudes >60°. According to Li et al. (2008), only West Africa (at 715 Ma) and Baltica (at 635 Ma) had as much as half their respective areas at latitudes >60°. Nevertheless, the sparse distribution of glacigenic deposits on the most poleward continents may reflect conditions so cold and dry that ice sheets failed to thicken sufficiently to be dynamic and transport rock debris. The 635 Ma distribution (Fig. 7B) displays a secondary minimum in the subtropics, similar to the distribution of precipitation minus evaporation related to the Hadley circulation, a not unreasonable predictor of ice-sheet mass-balance on an ice-covered planet.

The distribution of Ediacaran glacigenic formations (Fig. 7A) is quite different. They occur disproportionately at high palaeolatitudes (>45°). This reflects the preponderance of high-latitude palaeocontinents and is consistent with regional-scale glaciation like the late Paleozoic and late Cenozoic. However, there are also four purported glacigenic formations at low palaeolatitudes, two of which occur in carbonate-bearing successions. The Luoquan Formation, on the southern margin of the North China craton bordering the Qinling orogenic belt (early Mesozoic), includes ice-contact tillites, glaciomarine diamictites, rhythmites with dropstones, outwash conglomerates and sandstones, and striated pavements and clasts (Guan et al., 1986). However, direct palaeomagnetic constraints are lacking (Zhang et al., 2006) and the palaeolatitude of the Luoquan glaciation could be greater than shown in Fig. 6. The Croles Hill diamictite in northwestern Tasmania occurs within a succession of mafic and felsic terrestrial volcanics (Calver et al., 2004). Diamictites are notoriously difficult to interpret in such settings because of the many volcanic-related processes that can produce matrix-supported diamictites (e.g., lahars) and because of the potential for mountain glaciers unrelated to global temperature minima. However, the proximity of its age of 582 Ma to that of the Gaskiers glaciation (Fig. 2) suggests that it did form at a time of glaciation. Perhaps the best candidates for low-latitude Ediacaran glaciation are the carbonate-associated Egan (Corkoran and George, 2001) and Hankalchough (Xiao et al., 2004) glaciations.

3.2. Polygonal sand-wedges

Polygonal fracture networks caused by thermal contraction cracking of frozen ground form poleward of 17° latitude on Earth and Mars today (Leffingwell, 1915; Lachenbruch, 1962; Black, 1976; Mellon, 1997). In the Neoproterozoic, periglacial sand-wedges occur in the Sturtian Port Askaig Formation (Spencer, 1971), the Marinoan Wilsonbreen (Chumakov, 1968; Harland et al., 1993), Smalfjord (Edwards, 1975), Jbéliat (Deynoux, 1982), Elatina (Williams and Tonkin, 1985; Williams, 1986, 2000; Schmidt and Williams, 1995), Storeelv (Hambrey and Spencer, 1987) and Bakoye (Deynoux et al., 1989) formations, and in the Ediacaran Moelv (Nystuen, 1976) and Luoquan (Guan et al. 1986) formations. These formations are identified on the palaeogeographic maps (Fig. 6) as stars with heavy black lines. With two exceptions, they all occur at palaeolatitudes greater than 30°, consistent with seasonal temperature change as the ultimate cause of the thermal stresses.

One exception is the Marinoan Elatina glaciation (Fig. 6B) in South Australia, where a permafrost block field, developed on Mesoproterozoic quartzite on the Stuart Shelf of the Gawler Craton, is overlain by a synglacial aeolian sand sheet, the Whyalla Formation (Williams, 1998). Wedges composed of Whyalla sandstone taper downwards into the block field to an average depth of ~2.5 m and a second generation of wedges is developed within the sand sheet near its base (Williams and Tonkin, 1985; Williams, 1986). Reliable palaeomagnetic data from the Elatina Formation and its cap dolostone, the Nuccaleena Formation, place the sand-wedges at less than 15° palaeolatitude (Embleton and Williams, 1986; Schmidt and Williams, 1995; Sohl et al., 1999; Raub and Evans, 2006). Because seasonality close to the equator is weak with small orbital obliquity, the existence of the Elatina sand-wedges provides empirical support for the hypothesis that preferential low-latitude glaciation in the Neoproterozoic was a response to a large orbital obliquity at that time (Williams, 1975; Schmidt and Williams, 1995; Williams, 2000). The large-obliquity hypothesis, which requires a rapid decrease in obliquity before the Cambrian, has been criticized on the grounds of orbital mechanics (Néron de Surgy and Laskar, 1997; Pais et al., 1999) and the meridional distribution of climate-sensitive sedimentary indicators (Evans, 2006; see also sections 3.0 and 4.1 of this work). Alternatively, Maloof et al. (2002) suggest that the Elatina sand-wedges formed in permanently frozen ground as a result of diurnal temperature oscillations, with the depth of crack propagation greatly exceeding the depth of the thermal fluctuations because of extremely brittle soil behaviour under the conditions of a snowball earth.

The other exception is the Ediacaran Luoquan Formation (Fig. 6A) in North China, where wedges of fine gravel and sand ~1.0 m deep are described in one section (Guan et al., 1986). As the Ediacaran glaciation is unlikely to have been a snowball earth because of its short duration (Fig. 2), the explanation of Maloof et al. (2002) should not apply. The Ediacaran palaeolatitude of North China is not well constrained (Zhang et al., 2006), however, and may have been greater than shown in Fig. 6.

3.3. Syn-glacial iron- and iron-manganese formations

The occurrence of extensive Fe_2O_3 and Fe_2O_3-MnO_2 deposits, uniquely associated in the post-Palaeoproterozoic sedimentary record with Cryogenian glaciomarine deposits, has long been viewed as supporting the existence of an ice-covered ocean (Martin, 1965; Kirschvink, 1992; Klein and Beukes, 1993; Canfield and Raiswell, 1999; Hoffman and Schrag, 2002; Klein and Ladeira, 2004; Kump and Seyfried, 2005). Even assuming that air-sea gas exchange through cracks in dynamic sea-ice maintained equilibrium with respect to CO_2 on geological time-scales, the rate of O_2 uptake was likely insufficient to offset O_2 consumption related to the discharge of reduced species at hydrothermal vents. Consequently, deep waters would become anoxic, allowing reduced Fe to be transported widely in solution. Fe-rich waters would be possible if H_2S production was low because of diminished input of SO_4^{2-} from the glaciated continents (Raiswell and Canfield, 1999) and because of lowered S:Fe ratios in hydrothermal vent fluids due to the fall in hydrostatic pressure resulting from glacioeustatic drawdown (Kump and Seyfried, 2005; Hoffman et al., 2007, Hoffman, 2008). Canfield et al. (2008) have recently suggested that ocean deep waters were Fe-rich during most of late Neoproterozoic time, but this begs the question why no banded Fe-formations occur in non-glacial sequences of that age.

The occurrence of Fe- and Fe-Mn-deposits within glaciomarine sequences, including ice-proximal sequences (Martin, 1965; Whitten, 1970; Young, 1976; Klein and Beukes, 1993; Trompette et al., 1998; Klein and Ladeira, 2004), suggests that precipitation of the Fe_2O_3 precursor and MnO_2 occurred close to ice grounding-lines. The O_2 responsible for their precipitation could have been supplied by subglacial meltwater discharges (Hoffman, 2005), assuming that the contemporary atmosphere and therefore air bubbles in glacial ice contained significant concentrations of O_2. If atmospheric O_2 was drawn down during glaciation by subaerial volcanic emissions, then hydrogen peroxide (H_2O_2) entrained in glacial ice as a result of ultra-violet irradiation could have supplied the oxidant for Fe- and Fe-Mn deposits (Liang et al., 2006).

Sedimentary Fe_2O_3 deposits occur within the Sturtian Rapitan and Surprise diamictites of the North American Cordillera, the Kaigas of Namibia and the Tany of the Urals; Fe_2O_3 + MnO_2 deposits within the Sturtian Sturt, Chang'an and Chuos diamictites of Australia, South China and Namibia, respectively, and the Marinoan Puga diamictite of Brazil. Fe_2O_3 deposits also occur in the glacigenic Rizu Formation of central Iran. Its age is uncertain but we tentatively assign it to the Marinoan because of the presence of a cap dolostone that is strongly depeleted in $\delta^{13}C$ (Kianian and Khakzad, 2008). Eight of the nine deposits lie within 30° and half within 15° of the palaeoequator (Fig. 6). Thus they all occur where subglacial meltwater production should have been greatest. Although local sources of volcanogenic Fe have been invoked by some authors (Young, 1976, 2002), volcanic rocks are rare or absent in the glacigenic formations hosting Fe or Fe-Mn deposits. No Fe or Fe-Mn deposits are associated with Ediacaran glaciations, consistent with a limited extent of sea-ice at that time.

3.4. Syn-glacial sand seas

Marinoan syn-glacial aeolian sand seas (ergs) are well described by Deynoux et al. (1987) from the Bakoye Formation of Mali and by Willliams (1998) from the Whyalla Sandstone (Elatina glaciation) of South Australia (Fig. 6B). Reliable palaeomagnetic data place the Elatina within 15° of the palaeoequator (Embleton and Williams, 1986; Schmidt and Williams, 1995; Sohl et al., 1999; Raub and Evans, 2006), in the northern hemisphere in conventional reconstructions (Williams, 1998; Li et al., 2008). There are no reliable Cryogenian palaeomagnetic data for West Africa and its declination and palaeolatitude ~40° S (Fig. 6B) rest on the questionable assumption that the Rockelide orogen connecting it to Amazonia was sutured by 635 Ma (Li et al., 2008).

Palaeowind directions inferred from aeolian foreset inclinations were from the northwest in South Australia (Williams, 1998) and southeast in Mali (Deynoux et al., 1989) assuming the reconstruction (Fig. 6B) to be correct. Neither wind direction would be predicted from the palaeogeography. Easterly trade winds would be predicted for tropical South Australia given open water to the east; mid-latitude westerlies would be predicted for West Africa given open water in that direction (Fig. 6B). We tentatively suggest that katabatic winds prevailed in both areas and that their directions were dictated by the descent of cold air off the adjacent ice sheets, which were centered over northwestern Australia (Perry and Roberts, 1968; Preiss, 1987) and northern West Africa (Deynoux et al., 1989), respectively.

4. Palaeogeography of post-glacial cap carbonates

4.1. Syn-deglacial 'cap dolostones'

A unique feature of the Marinoan glaciation was the deposition globally of transgressive 'cap dolostones' (Kennedy, 1996) during the glacioeustatic flooding of continental margins and inland seas as ice-sheets receded (Hoffman et al., 2007). These pale yellowish or pinkish dolostones are typically well-laminated and were deposited as sand- and silt-sized peloids and micropeloids (James et al., 2001; Xiao et al., 2004). Characteristic sedimentary structures include low-angle cross-lamination, giant wave ripples (Allen and Hoffman, 2005a) and stromatolite bioherms containing 'geoplumb' (paleovertical) tubes filled by laminated micropeloidal sediment and/or void-filling cement (Cloud et al., 1974; Corsetti and Grotzinger, 2005). Cap dolostones in West Africa and South China are top-truncated by subaerial exposure surfaces and contain 'tepee' structures and 'tepee breccias' (Assereto and Kendall, 1971, 1977; Kendall and

Warren, 1987) with early diagenetic crustose barite cement (Jiang et al., 2006; Shields et al., 2007a, b). The lack of accommodation space in West Africa and South China likely stems from an absence of tectonic subsidence during the glacial period (Hoffman and Schrag, 2002). Cap dolostones have a global average thickness of ~18 m and their deposition on the timescale of ice-sheet melting implies sedimentation rates on the order of 1.0 cm.yr^{-1} (Hoffman et al., 2007). The alkalinity flux responsible for cap dolostone sedimentation is attributed to carbonate weathering (Higgins and Schrag, 2003) augmented by glacioeustatic effects on carbonate saturation (Kennedy, 1996; Ridgwell et al., 2003), and anaerobic methane oxidation (Kennedy et al., 2001). Transgressive cap carbonates, as distinct from high-stand cap carbonates, are not found above Sturtian glacigenic deposits, suggesting that critical oversaturation was not achieved until after those ice-sheets had completely disappeared (Hoffman and Schrag, 2002).

In Fig. 8, we plot the thickness of Marinoan cap dolostones (based on data compiled in Table 1 of Hoffman et al., 2007) as a function of palaeolatitude. Despite considerable scatter, there is a discernable correlation of maximum thickness with palaeolatitude. All those thicker than 12 m, ranging from 24 to 175 m, were deposited at palaeolatitudes lower than 27°. Conversely, all those deposited at palaeolatitudes higher than 37° are less than 6 m thick. The correlation could be explained in different ways. First, the rate of sedimentation and therefore the thickness should be a function of temperature because of the temperature-dependence of dolomite (or calcite) saturation: the stronger dependence on pressure would not be a factor for these shallow-water deposits. Second, on the assumption that ice-sheets receded poleward during deglaciation, middle-latitude areas should have been ice-free for a shorter time interval before the end of the glacioeustatic transgression compared with low-latitude areas. This effect should have been particularly important given the absence of high-latitude continents in the Cryogenian (Fig. 6). And third, the ice-free fraction of the glacioeustatic rise should have been greatest close to the palaeo-equator, thereby maximizing accommodation at low latitudes and minimizing it at high latitudes.

According to all three explanations, the observed correlation (Fig. 8) argues against a reverse meridional temperature gradient (i.e., equator colder than the poles) due to large orbital obliquity, hypothesized to account for low-latitude glaciation (Williams, 1975; Williams and Schmidt, 2004). Our data therefore support the conclusion of Evans (2006), based on the palaeolatitudes of evaporite deposits over geologic time, that the Earth has had a normal meridional temperature gradient and therefore a low (<54 degrees) orbital obliquity since Palaeoproterozoic time.

4.2. Azimuthal orientations of giant wave ripples

Distinctive sedimentary bedforms in Marinoan cap dolostones are 'giant wave ripples' (Allen and Hoffman, 2005a). These strongly aggradational structures have trochoidal profiles (*i.e.,* curved troughs and sharp, near-symmetrical crests) with bidirectional cross-stratification in their crestal regions. Their synoptic relief, crest-to-trough, is 20-40 cm and the crestlines are spaced 1.5-5.5 m apart (see data in Allen and Hoffman, 2005a). Individual ripple trains aggrade through a stratigraphic thickness of <1.4 m. They initiate from a plane bed and die out by onlap or truncation. The crests develop sigmoidally, climbing obliquely near the base, vertically in the main stage and obliquely again near the top. Although they were originally described as tepee structures, their crestlines in plan view are consistently straight and parallel (Aitken, 1991; James et al., 2001), not polygonal like those of true tepee structures (Assereto and Kendall, 1971, 1977; Kendall and Warren, 1987), which originate by lateral expansion due to the force of crystallization of evaporative cements precipitated in supratidal settings. In addition, synsedimentary breccias and associated void-filling cements, which are diagnostic features of true tepee structures (Assereto and Kendall, 1971, 1977; Kendall and Warren, 1987), are not associated with giant wave ripples. As noted above, true tepee structures and tepee breccias do occur in cap dolostones in West Africa (Hoffman and Schrag, 2002; Shields et al., 2007a, b) and South China (Jiang et al., 2006), but they are quite distinct from the giant wave ripples found elsewhere.

Gammon et al. (2005) interpreted tepee structures in the Nuccaleena cap dolostone at Parachilna Gorge, South Australia, in terms of syn-sedimentary faulting because of decreases in apparent fault displacement up-section. However, the faults are oriented perpendicular to bedding and could not therefore have formed in response to bedding-parallel extension or contraction. Fault slip was probably at a high angle to the plane of the outcrop (i.e., strike-slip if syndepositional), in which case the 2-dimensional analysis (Gammon et al., 2005) is innappropriate for the 3-dimensional displacement problem: uniform displacement of warped strata could easily result in variable offsets up-section. Moreover, most intrastratal wave structures in the Nuccaleena Formation are not associated with faults (Fig. 9).

Allen and Hoffman (2005a) relate the bedforms to surface gravity waves and attribute their near-symmetrical form, trochoidal profile, bidirectional internal cross-stratification and chevron-type upbuilding in the crestal region to oscillatory flow with flow separation over the bedform crest with each half-cycle of the wave motion. Their hydrodynamic analysis suggests that the bedforms formed at water depths of 200-400 m under the influence of long-period (maximum 21-30 seconds) waves generated by sustained wind velocities exceeding 20 $m.s^{-1}$ in basins of unlimited fetch (Allen and Hoffman, 2005a). In comparison, zonal wind velocities in today's oceans (e.g., trade winds) average ~7 $m.s^{-1}$. As giant wave ripples are observed in cap dolostones on at least 8 palaeocontinents (Table 2), but have not been reported elsewhere in the stratigraphic column, Allen and Hoffman (2005a) ascribe their occurrence to extraordinary meteorological conditions during ice-sheet retreat following a snowball Earth. Jerolmack and Mohrig (2005), in contrast, suggest that giant wave ripples formed at depths of 20-40 m under the influence of hurricanes. Because hurricanes are small in areal extent, successive hurricanes should intersect a coast at different locations, producing variable wind and wave conditions in successive events. In contrast, Allen and Hoffman (2005b) noted that where successive ripple trains are observed, their crestal azimuths do not differ by more than 15°. This observation supports an origin by sustained zonal winds.

In Fig. 10, we test the zonal wind hypothesis by plotting the azimuthal orientations of giant wave ripple crests (Table 2) on the palaeogeographic map for 635 Ma (Li et al., 2008). We summarize the results in rose diagrams representing the individual measurements (n=68) and the mean orientations for each region (n=12). As there are no independent (i.e., palaeomagnetic) data constraining the orientation of the Tuva-Mongolia microcontinent, we do not include the data (Table 2) from that region in our compilation. The overall mean azimuths are 001-181° (95% confidence interval = 20°) and 173-353° (95% confidence interval = 48°). Notably absent are azimuths between 056-236° and 121-301° (Fig. 10). Assuming the ripple crests are oriented perpendicular to the oscillation directions in the water column incited by the surface winds, the observed orientations are consistent with zonal (easterly) winds, given that most of the data come from palaeolatitudes below 30° (Fig. 10). Individual measurements show little evidence of wave refraction (crests are typically orientated at high angles to inferred shorelines and slope contours), so the dispersion in the data may reflect a combination of palaeotopographic effects on surface winds, Ekman forcing in subsurface waters and errors in the palaeogeographic reconstruction. Ekman forcing might possibly account for the deviation from a N-S orientation (i.e., 173-353°) of the regional means given the strong southern-hemisphere bias in their palaeogeographic distribution (Fig. 10). In any event, the non-random distribution of azimuthal orientations is more consistent with zonal winds than with hurricanes as the agent responsible for the giant wave ripples.

4.3. Facies of cap-carbonate sequences

'Cap-carbonate sequences' (Hoffman and Schrag, 2002) refer to depositional sequences initiated by glacioeustatic flooding and ultimately accommodated by syn-glacial erosion and subsidence. Cap dolostones are the transgressive tracts of cap-carbonate sequences. The maximum flood and highstand tracts of cap-carbonate sequences are variable in facies, carbonate and/or siliciclastic (Hoffman and Schrag 2002). In Fig. 11, we categorize the maximum flood and lower highstand facies of Marinoan cap-carbonate sequences globally: distinguishing organic-rich and organic-poor siliciclastic- and carbonate-dominated facies. The siliciclastic- and carbonate-dominated designations differ from those in Fig. 6, which relate to the pre-glacial successions. We acknowledge that some sequences have likely been misclassified because of surficial weathering causing organic degradation. The Masirah Bay Formation, for example, is organic-poor in outcrop, but a significant petroleum source rock in the subsurface. Perhaps this is why the distribution of organic-rich and organic-poor cap carbonates makes little sense (Fig. 11). The only meaningful correlation appears to be the limitation of carbonate-rich sequences to palaeolatitudes less than 35°, similar to their distribution in pre-glacial successions (Fig. 6).

5. Conclusions

Cryogenian glacigenic deposits occur at palaeolatitudes <60° and disproportionately at <45°, where most of the palaeocontinents then resided (Fig. 12). Ediacaran diamictites occur predominantly at palaeolatitudes >45° and some closest to the palaeoequator may be non-glacial in origin or mislocated. Glacigenic formations within carbonate-dominated and carbonate-bearing successions all formed within 35° of the palaeoequator, supporting the validity of the palaeogeographic maps (Li et al., 2008), which were constructed strictly according to non-climatological criteria. Most glacigenic Fe and Fe-Mn deposits occur at palaeolatitudes <30°, whereas most polygonal sand-wedges formed at palaeolatitudes >30°. The maximum thicknesses of syn-deglacial cap dolostones decrease with palaeolatitude, which along with the meridional distribution of carbonate-bearing successions generally supports a low-obliquity orbit with warmer tropics and colder poles. Meridional (N-S) mean orientations of the crestlines of giant wave ripples in cap dolostones and the absence of zonal (W-E) orientations supports their formation by zonal wind-driven waves and not by hurricanes. The palaeogeographic maps (Li et al., 2008), although lacking palaeotopography, provide a suitable starting point for general circulation models of Neoproterozoic palaeoclimate.

Acknowledgements

An ArcView extension written by Sergei Pisarevsky was used for rotating geographic information using Euler poles. The paper was written while PFH was supported by a Harvard Club of Australia Fellowship, hosted by The School of Earth and Environmental Sciences, The University of Adelaide (Adelaide, South Australia), and by Curtin University of Technology (Perth, Western Australia). ZXL was supported by ARC Discovery Project DP0770228. We thank Samuel A. Bowring for unpublished geochronological constraints on the Gaskers glaciation, Francis A. Macdonald for unpublished data on giant wave ripples, Julius Sovetov for information on glacigenic sequences of the Siberian craton, and Bei Xu and co-authors for their preprint. David A.D. Evans, Francis A. Macdonald and Wolfgang Preiss made valuable comments on the manuscript, as did critical reviews by Graham Shields and Paul Link. This is TIGeR publication #000.

References

Aalto, K.R., 1981. The Late Precambrian Toby Formation of British Columbia, Idaho and Washington. In: Hambrey, M.J., Harland, W.B. (Eds.), Earth's Pre-Pleistocene Glacial Record. Cambridge University Press, Cambridge, pp. 731-735.

Aitken, J.D., 1991. The Ice Brook Formation and post-Rapitan, late Proterozoic glaciation, Mackenzie Mountains, Northwest Territories. Geological Survey of Canada Bulletin 404, 43 p.

Allen, P.A., Hoffman, P.F., 2005a. Extreme winds and waves in the aftermath of a Neoproterozoic glaciation. Nature 433, 123-127.

Allen, P.A., Hoffman, P.F., 2005b. Formation of Precambrian sediment ripples: Reply to Jerolmack, D.J., Mohrig, D. Nature, 10.1038/nature04025.

Allen, P., Leather, J., Brasier, M.D., 2004. The Neoproterozoic Fiq glaciation and its aftermath, Huqf Supergroup of Oman. Basin Research 16, 507-534.

Allison, C.W., Young, G.M., Yeo, G.M., Delaney, G.D., 1981. Glacigenic rocks of the Upper Tindir Group, east-central Alaska. In: Hambrey, M.J., Harland, W.B. (Eds.), Earth's Pre-Pleistocene Glacial Record. Cambridge University Press, Cambridge, pp. 720-723.

Alvarenga, C.J.S. de, Trompette, R., 1992. Glacially influenced sedimentation in the Later Proterozoic of the Paraguay belt (mato Grosso, Brazil). Palaeogeography, Palaeoclimatology, Palaeoecology 92, 85-105.

Alvarenga, C.J.S. de, Figueiredo, M.F., Babinki, M., Pinho, F.E.C., 2007. Glacial diamictites of Serra Azul Formation (Ediacaran, Paraguay belt): Evidence of the Gaskiers glacial event in Brazil. Journal of South American Earth Sciences 23, 236-241.

Assereto, R.L., Kendall, C.St.G., 1971. Megapolygons in Ladinian limestones of the Triassic of the Southern Alps: evidence of deformation by penecontemporaneous desiccation and cementation. Journal of Sedimentary Petrology 41, 715-723.

Assereto, R.L., Kendall, C.St.G., 1977. Nature, origin and classification of peritidal tepee structures and related breccias. Sedimentology 24, 153-210.

Black, R., 1976. Periglacial features indicative of permafrost: ice and soil wedges. Quaternary Research 6, 3-26.

Blackett, P.M.S., 1961. Comparison of ancient climates with the ancient latitudes deduced from rock magnetic measurements. Proceedings of the Royal Society of London, Series A, 263, 1-30.

Borg, G., Kärner, K., Buxton, M., Armstrong, R., van der Merwe, S.W., 2003. Geology of the Skorpion supergene zinc deposit, southern Namibia. Economic Geology 98, 749-771.

Bowring, S.A., Myrow, P., Landing, E., Ramezani, J., Grotzinger, J.P., 2003. Geochronological constraints on terminal Neoproterozoic events and the rise of metazoans. European Geophysical Union Annual Meeting, Nice 2003, Geophysical Research Abstracts 5, p. 13219.

Bowring, S.A., Grotzinger, J.P., Condon, D.J., Ramezani, J., Newall, M. 2007. Geochronologic constraints on the chronostratigraphic framework of the Neoproterozoic Huqf Supergroup, Sultanate of Oman. American Journal of Science 307, 1097-1145.

Brasier, M., McCarron, G., Tucker, R., Leather, J., Allen, P., Shields, G., 2000. New U-Pb zircon dates for the Neoproterozoic Gubrah glaciation and for the top of the Huqf Supergroup, Oman. Geology 28, 175-178.

Briden, J.C., 1970. Palaeolatitude distribution of precipitated sediments. In: Runcorn, S.K. (Ed.), Palaeogeophysics. Academic Press, London, pp. 437-444.

Briden, J.C., Irving, E., 1964. Palaeolatitude spectra of sedimentary palaeoclimatic indicators. In: Nairn, A.E.M. (Ed.), Problems in Palaeoclimatology. John Wiley and Sons, New York, pp. 199-224.

Cahen, L., Lepersonne, J., 1981. Proterozoic diamictites of Lower Zaire. In: Hambrey, M.J., Harland, W.B. (Eds.) Earth's Pre-Pleistocene Glacial Record. Cambridge University Press, Cambridge, pp. 153-157.

Caldeira, K., Kasting, J.F., 1992. Susceptibility of the early Earth to irreversible glaciation caused by carbon dioxide clouds. Nature 359, 226-228.

Calver, C.R., 1998. Isotope stratigraphy of the Neoproterozoic Togari Group, Tasmania. Australian Journal of Earth Sciences 45, 865-874.

Calver, C.R., Walter, M.R., 2000. The late Neoproterozoic Grassy Group of King Island, Tasmania: correlation and palaeogeographic significance. Precambrian Research 100, 299-312.

Calver, C.R., Black, L.P., Everard, J.L., Seymour, D.B., 2004. U-Pb zircon age constraints on late Neoproterozoic glaciation in Tasmania. Geology 32, 893-896, doi: 10.1130/G20713.1

Canfield, D.E., Raiswell, R., 1999. The evolution of the sulfur cycle. American Journal of Science 299, 697-723.

Canfield, D.E., Poulton, S.W., Knoll, A.H., Narbonne, G.M., Ross, G., Goldberg, T., Strauss, H., 2008. Ferruginous conditions dominated later Neoproterozoic deep-water chemistry. Science 321, 949-952.

Cloud, P., Wright, L.A., Williams, E.G., Diehl, P., Walter, M.R., 1974. Giant stromatolites and associated vertical tubes from the upper Proterozoic Noonday Dolomite, Death Valley region, eastern California. Geological Society of America Bulletin 85, 1869-1882.

Chew, D., Kirkland, C., Schaltegger, U., Goodhue, R., 2007. Neoproterozoic glaciation in the Proto-Andes: Tectonic implications and global correlation. Geology 35, 1095-1098.

Chumakov, N.M., 1968. On the character of the Late Precambrian glaciation of Spitsbergen (in Russian). Doklady Akademia Nauk SSSR, Geology Series 180, 1446-1449.

Chumakov, N.M., 1978. Precambrian tillites and tilloids (in Russian). Nauka, Moscow.

Chumakov, N.M., 2004. Climates and climate zonality of the Vendian: geological evidence. In: Vickers-Rich, P., Komarower, P. (Eds.), The Rise and Fall of the Ediacaran Biota. Geological Society of London, Special Publications 286, pp. 15-26.

Coats, R.P., Preiss, W.V., 1980. Stratigraphic and geochronological reinterpretation of Late Proterozoic glaciogenic sequences in the Kimberley Region, Western Australia. Precambrian Research 13, 181-208.

Condon, D., Zhu, M., Bowring, S.A., Wang, W., Yang, A., Jin, Y., 2005. U-Pb ages from the Neoproterozoic Doushantuo Formation, China. Science 308, 95-98.

Corkeron, M.L., George, A.D., 2001. Glacial incursion on a Neoproterozoic carbonate platform in the Kimberley region, Australia. Geological Society of America Bulletin 113, 1121-1132.

Corsetti, F.A., Grotzinger, J.P., 2005. Origin and significance of tube structures in Neoproterozoic post-glacial cap carbonates: example from Noonday Dolomite, Death Valley, United States. Palaios 20, 348-363.

Dempster, T.J., Rogers, G., Tanner, P.W.G., Bluck, B.J., Muir, R.J., Redwood, S.D., Ireland, T.E., Patterson, B.A., 2002. Timing of deposition, orogenesis and glaciation within the Dalradian rocks of Scotland. Journal of the Geological Society, London 159, 83-94.

Deynoux, M., 1982. Periglacial polygonal structures and sand wedges in the late Precambrian glacial formations of the Taoudeni Basin in Adrar of Mauretania (West Africa). Palaeogeography, Palaeoclimatology, Palaeoecology 39, 55-70.

Deynoux, M., 1985. Terrestrial or waterlain glacial diamictites? Three case studies from the late Proterozoic and late Ordovician glacial drifts in West Africa. Palaeogeography, Palaeoclimatology, Palaeoecology 51, 97-141.

Deynoux, M., Kocurek, G., Proust, J.N., 1989. Late Proterozoic periglacial aeolian deposits on the West African Platform, Taoudeni Basin, western Mali. Sedimentology 36, 531-549.

Deynoux, M., Proust, J.N., Simon, B., 1991. Late Proterozoic glacially controlled shelf sequences in Western Mali (West Africa). Journal of African Earth Sciences 12, 181-198.

Donnadieu, Y., Goddéris, Y., Ramstein, G., Nédélec, A., Meert, J., 2004. A 'snowball Earth' climate triggered by continental break-up through changes in runoff. Nature 428, 303-306.
Donnadieu, Y., Ramstein, G., Goddéris, Y., Fluteau, F., 2004. Global tectonic setting and climate of the Late Neoproterozoic: a climate-geochemical coupled study. In: Jenkins, G.S., McMenamin, M.A.S., McKey, C.P., Sohl, L. (Eds.), The Extreme Proterozoic: Geology, Geochemistry, and Climate. Geophysical Monograph 146, American Geophysical Union, Washington, DC., pp. 79-89.
Dunn, P.R., Thomson, B.P., Rankama, K., 1971. Late Pre-Cambrian glaciation in Australia as a stratigraphic boundary. Nature 231, 498-502.
Edwards, M.B., 1975. Glacial retreat sedimentation in the Smalfjord Formation, late Precambrian, North Norway. Sedimentology 22, 75-94.
Edwards, M.B., 1984. Sedimentology of the Upper Proterozoic glacial record, Vestertana Group, Finnmark, North Norway. Norges Geologiske Undersøkelse Bulletin 394, 76 p.
Embleton, B.J.J., Williams, G.E., 1986. Low latitude of deposition for late Precambrian periglacial varvites in South Australia: implications for palaeoclimatology. Earth and Planetary Science Letters 79, 419-430.
Evans, D.A.D., 2000. Stratigraphic, geochronological, and paleomagnetic constraints upon the Neoproterozoic climatic paradox. American Journal of Science 300, 347-433.
Evans, D.A.D., 2003. A fundamental Precambrian–Phanerozoic shift in earth's glacial style? Tectonophysics 375, 353-385.
Evans, D.A.D., 2006. Proterozoic low orbital obliquity and axial-dipolar geomagnetic field from evaporite palaeolatitudes. Nature 444, 51-55.
Eyles, N., Eyles, C.H., 1989. Glacially-influenced deep-marine sedimentation of the Late Precambrian Gaskiers Formation, Newfoundland, Canada. Sedimentology 36, 601-620.
Fanning, C.M., Link, P.K., 2004. U-Pb SHRIMP ages of Neoproterozoic (Sturtian) glaciogenic Pocatello Formation, southeastern Idaho. Geology 32, 881-884, doi:10.1130/G20609.1
Fanning, C.M., Link, P.K., 2008. Age constraints for the Sturtian glaciation: data from the Adelaide Geosyncline, South Australia and Pocatello Formation, Idaho, USA. Geological Society of Australia Abstracts, No. 91, Selwyn Symposium 2008, Melbourne, 57-62.
Frimmel, H.E., Fölling, P.G., Eriksson, P.G., 2002. Neoproterozoic tectonic and climatic evolution recorded in the Gariep Belt, Namibia and South Africa. Basin Research 14, 55-67.
Frimmel, H.W., Klötzi, U.S., Siegfried, P.R., 1996. New Pb-Pb single zircon age constraints on the timing of Neoproterozoic glaciation and continental break-up in Namibia. Journal of Geology 103, 313-326.
Gammon, P.R., McKirdy, D.M., Smith, H.D., 2005. The timing and environment of tepee formation in a Marinoan cap carbonate. Sedimentary Geology 177, 195-208.
Goddéris, Y., Donnadieu, Y., Nédélec, A., Dupré, B., Dessert, C., Grard, A., Ramstein, G., Francois, L.M., 2003. The Sturtian 'snowball' glaciation: fire and ice. Earth and Planetary Science Letters 211, 1-12.

Graindor, M.J., 1964. Les tillites ante-cambriennes de Normandie. Geologische Rundschau 54, 61-83.

Guan, B., Ruitang, W., Hambrey, M.B., Geng, W., 1986. Glacial sediments and erosional pavements near the Cambrian-Precambrian boundary in western Henan Province, China. Journal of the Geological Society, London 143, 311-323.

Halliday, A.N., Graham, C.M., Aftalon, M. Dymoke, P.L., 1989. The depositional age of the Dalradian Supergroup: U-Pb and Sm-Nd isotopic studies of the Tayvallich volcanics, Scotland. Journal of the Geological Society, London 146, 3-6.

Halverson, G.P., 2006. A Neoproterozoic chronology. In: Xiao, S., Kaufman, A.J. (Eds.) Neoproterozoic Geobiology and Paleobiology. Springer, Dordrecht, pp. 231-271.

Hamdi, B., 1992. Late Precambrian glacial deposits in central Iran. 29th International Geological Congress Abstracts 2, 263, Kyoto, Japan.

Hambrey, M.J., Spencer, A.M., 1987. Late Precambrian glaciation of central East Greenland. Meddelelser om Grønland, Geoscience 19, 50 p.

Harland, W.B., Hambrey, M.J., Waddams, P., 1993. Vendian Geology of Svalbard. Norsk-Polarinstitutt Skrifter 193, 150 p.

Higgins, J.A., Schrag, D.P., 2003. Aftermath of a snowball Earth. Geophysics, Geochemistry, Geosystems 4, 10.1029/2002GC000403.

Hoffman, P.F., 2005. 28th DeBeers Alex. Du Toit Memorial Lecture: On Cryogenian (Neoproterozoic) ice-sheet dynamics and the limitations of the glacial sedimentary record. South African Journal of Geology 108, 557-576.

Hoffman, P.F., 2008. Large glacioeustatic changes during the Ghaub glaciation (635 Ma) and its syn-deglacial cap dolostone, Otavi carbonate platform, northern Namibia. 33rd International Geological Congress, Oslo, 2008, Abstracts, Session CGC-04.

Hoffman, P.F., 2009. Pan-glacial—a third state in the climate system. Geology Today (in press).

Hoffman, P.F., Halverson, G.P. 2008. Otavi Group of the western Northern Platform, the Eastern Kaoko Zone and the western Northern Margin Zone. In: Miller, R. McG. (Ed.), The Geology of Namibia, vol. 2. Handbook of the Geological Survey of Namibia, Windhoek, pp. 13.69-13.136.

Hoffman, P.F., Schrag, D.P., 2002. The snowball Earth hypothesis: testing the limits of global change. Terra Nova 14, 129-155.

Hoffman, P.F., Halverson, G.P., Domack, E.W., Husson, J.M., Higgins, J.A., Schrag, D.P., 2007. Are basal Ediacaran (635 Ma) post-glacial "cap dolostones" diachronous? Earth and Planetary Science Letters 258, 114-131.

Hoffman, P.F., Hawkins, D.P., Isachsen, C.E., Bowring, S.A. 1996. Precise U-Pb zircon ages for early Damaran magmatism in the Summas Mountains and Welwitschia Inlier, northern Damara belt, Namibia. Communications of the Geological Survey of Namibia, 11, 47-52.

Hoffmann, K.-H., Condon, D.J., Bowring, S.A., Crowley, J.L., 2004. U-Pb zircon date from the Neoproterozoic Ghaub Formation, Namibia: constraints on Marinoan glaciation. Geology 32, 817-820.

Holland, T.H., 1908. On the occurrence of striated boulders in the Blaini Formation of Simla, with a discussion of the geological age of the beds. Records of the Geological Survey of India 37(3), 129-135.

Hyde, W.T., Crowley, T.J., Baum, S.K., Peltier, W.R., 2000. Neoproterozoic ‘snowball Earth’ simulations with a coupled climate/ice-sheet model. Nature 405, 425-429.
Ireland, T.R., Flöttman, T., Fanning, C.M., Gibson, G.M., Preiss, W.V., 1998. Development of the early Paleozoic Pacific margin of Gondwana from detrital-zircon ages across the Delamerian orogen. Geology 26, 243-246.
James, N.P., Narbonne, G.M., Kyser, T.K., 2001. Late Neoproterozoic cap carbonates: Mackenzie Mountains, northwestern Canada: precipitation and global glacial meltdown. Canadian Journal of Earth Sciences 38, 1229-1262.
Jerolmack, D.J., Mohrig, D., 2005. Formation of Precambrian sediment ripples: Arising from P.A. Allen, P.F. Hoffman Nature 433, 123-127 (2005).
Jiang, G., Kennedy, M.J., Christie-Blick, N., Wu, H., Zhang, S., 2006. Stratigraphy, sedimentary structures, and textures of the late Neoproterozoic Doushantuo cap carbonate in South China. Journal of Sedimentary Research 76, 978-995.
Kendall, B.S., Creaser, R.A., Selby, D., 2006. Re-Os geochronology of postglacial black shales in Australia: constraints on the timing of "Sturtian" glaciation. Geology 34, 729-732.
Kendall, C.St.G., Warren, J., 1987. A review of the origin and setting of tepees and their associated fabrics. Sedimentology 34, 1007-1028.
Kennedy, M.J., 1996. Stratigraphy, sedimentology, and isotopic geochemistry of Australian Neoproterozoic postglacial cap dolostones: deglaciation, $\delta^{13}C$ excursions, and carbonate precipitation. Journal of Sedimentary Research 66, 1050-1064.
Kennedy, M.J., Christie-Blick, N., Sohl, L.E., 2001. Are Proterozoic cap carbonates and isotopic excursions a record of gas hydrate destabilization following Earth’s coldest intervals? Geology 29, 443-446.
Kennedy, M.J., Runnegar, B., Prave, A.R., Hoffmann, K.-H., Arthur, M.A., 1998. Two or four Neoproterozoic glaciations? Geology 26, 1059-1063.
Key, R.M., Liyungu, A.K., Njamu, F.M., Somwe, V., Banda, J., Mosley, P.N., Armstrong, R.A., 2001. The western arm of the Lufilian Arc in NW Zambia and its potential for copper mineralization. Journal of African Earth Sciences 33, 503-528.
Kianian, M., Khakzad, A., 2008. Geochemistry of glacigenic Neoproterozoic banded iron-formations from the Kerman District (Iran). 33rd International Geological Congress, Oslo, Abstracts, Session CGC-04.
Kiessling, W., 2001. Paleoclimatic significance of Phanerozoic reefs. Geology 29, 751-754.
Kirschvink, J.L., 1992. Late Proterozoic low-latitude glaciation: the snowball Earth. In: Schopf, J.W., Klein, C., (Eds.), The Proterozoic Biosphere, Cambridge University Press, Cambridge, pp. 51-52.
Klein, C., Ladeira, E.A., 2004. Geochemistry and mineralogy of Neoproterozoic banded iron-formations and some selected, siliceous manganese formations from the Urucum District, Mato Grosso do Sul, Brazil. Economic Geology 99, 1233-1244.
Klein, C., Beukes, N.J., 1993. Sedimentology and geochemistry of the glacigenic Late Proterozoic Rapitan iron-formation in Canada. Economic Geology 88, 542-565.
Kump, L.R., Seyfried, W.E., 2005. Hydrothermal Fe fluxes during the Precambrian: effect of low oceanic sulfate concentrations and low hydrostatic pressure on the composition of black smokers. Earth and Planetary Science Letters 235, 654-662.

Lachenbruch, A.H., 1962. Mechanics of thermal contraction cracks and ice-wedge polygons in permafrost. Geological Society of America Special Paper 70, Boulder, Colorado.

Leffingwell, E.deK., 1915. Ground-ice wedges: the dominant form of ground ice on the north coast of Alaska. Journal of Geology 23, 635-654.

Le Guerroué, E., Allen, P., Cozzi, A., 2005. Two distinct glacial successions in the Neoproterozoic of Oman. GeoArabia 10, 2005.

Li, Z.-X., Bogdanova, S.V., Collins, A.S., Davidson, A., De Waele, B., Ernst, R.E., Fitzsimons, I.C.W., Fuck, R.A., Gladkochub, D.P., Jacobs, J., Karlstrom, K.E., Lu, S., Natapov, L.M., Pease, V., Pisarevsky, S.A., Thrane, K., Vernikovsky, V., 2008. Assembly, configuration, and break-up history of Rodinia: A synthesis. Precambrian Research 160, 179-210.

Liang, M.-C., Hartman, H., Kopp, R.E., Kirschvink, J.L., Yung, Y.-L., 2006. Production of hydrogen peroxide in the atmosphere of the Snowball Earth and the origin of oxygenic photosynthesis. Proceedings of the National Academy of Sciences (USA) 103(50), 18896-18899.

Lindsay, J.F., Brasier, M.D., Shields, G., Khomentovsky, V.V., Bat-Ireedui, Y.A., 1996. Glacial facies associations in a Neoproterozoic back-arc setting, Zavkhan Basin, western Mongolia. Geological Magazine 133, 391-402.

Link, P.K., 1983. Glacial and tectonically influenced sedimentation in the Upper Proterozoic Pocatello Formation, southeastern Idaho. In: Miller, D.M., Todd, V.R., Howard, K.A. (Eds.), Tectonic and Stratigraphic Studies in the Eastern Great Basin. Geological Society of America Memoir 157, Boulder, CO, pp. 165-181.

Lund, K., Aleinikoff, J.N., Evans, K.V., Fanning, C.M., 2003. SHRIMP geochronology of Neoproterozoic Windermere Supergroup, central Idaho: implications for rifting of western Laurentia and synchroneity of Sturtian glacial deposits. Geological Society of America Bulletin 115, 349-372.

Macdonald, F.A., Jones, D.S., Schrag, D.P., 2009a. Stratigraphic and tectonic implications of a new glacial diamictite–cap carbonate doublet in southwestern Mongolia. Geology 37, 123-126.

Macdonald, F.A., McClelland, W.C., Schrag, D.P., Macdonald, W.P., 2009b. Neoproterozoic glaciation on a carbonate platform margin in Arctic Alaska and the origin of the North Slope subterrane. Geological Society of America Bulletin 121, 449-473.

Maloof, A.C., Kellogg, J.B., Anders, A.M., 2002. Neoproterozoic sand wedges: crack formation in frozen soils under diurnal forcing during a snowball Earth. Earth and Planetary Science Letters 204, 1-15.

Maloof, A.C., Halverson, G.P., Kirschvink, J.L., Schrag, D.P., Weiss, B.P., Hoffman, P.F., 2006. Combined paleomagnetic, isotopic and stratigraphic evidence for true polar wander from the Neoproterozoic Akademikerbreen Group, Svalbard. Geological Society of America Bulletin 118, 1099-1124.

Martin, H., 1965. Beobachtungen zum Problem der jung-präkambrischen Glazialen Ablagerungen in Südwestafrika (Observations concerning the problem of the late Precambrian glacial deposits in South West Africa). Geologische Rundschau 54, 115-127.

Mawson, D., Sprigg, R.C., 1950. Subdivision of the Adelaide System. Australian Journal of Science 13, 69-72.

McCay, G.A., Prave, A.R., Alsop, G.I., Fallick, A.E., 2006. Glacial trinity: Neoproterozoic Earth history within the British-Irish Caledonides. Geology 34, 909-912.

McMechan, M.E., 2000. Vreeland Diamictites—Neoproterozoic glaciogenic slope deposits, Rocky Mountains, northeast British Columbia. *Bulletin of Canadian* Petroleum Geology 48, 246-261.

Mellon, M., 1997. Small-scale polygonal features on Mars: seasonal thermal contraction cracks in permafrost. Journal of Geophysical Research 102, 25617-25628.

Miller, J.M.G., 1994. The Neoproterozoic Konnarock Formation, southern Virginia, USA: glaciolacustrine facies in a continental rift. In: Deynoux, M., Miller, J.M.G., Domack, E.W., Eyles, N., Fairchild, I.J., Young, G.M. (Eds.), Earth's Glacial Record. Cambridge University Press, Cambridge, pp. 47-59.

Miller, R. McG. (Ed.), 2008. The Geology of Namibia, vol. 2. Handbook of the Geological Survey of Namibia, Windhoek.

Misi, A., Azmy, K., Sial, A.N., Guimarães, J.T., Oliveira, F.B.M., 2008. The Neoproterozoic successions of the São Francisco craton and their glacigenic units in the Bambuí/Una and in the Vaza Barris/Miaba groups. 33rd International Geological Congress, Oslo, Abstracts, Session CGC-04.

Néron de Surgy, O., Laskar, J., 1997. On the long term evolution of the spin of the Earth. Astronomy and Astrophysics 318, 975-989.

Norin, E., 1937. Geology of the western Quruq Tagh, eastern Tien Shan. Reports of the Sino-Swedish Expedition III. Geology. Bokförlags Aktiebolaget Thule, Stockholm, 194 p.

Nystuen, J., 1976. Late Precambrian Moelv tillite deposited on a discontinuity surface associated with a fossil ice wedge, Rendalen, southern Norway. Norsk Geologiske Tidsskrift 56, 29-50.

Opdyke, B.N., Wilkinson, B.H., 1990. Paleolatitude distribution of Phanerozoic marine ooids and cements. Palaeogeography, Palaeoclimatology, Palaeoecology 78, 135-148.

Opdyke, N.D., 1962. Palaeoclimatology and continental drift. In: Runcorn, S.K. (Ed.), Continental Drift. Academic Press, New York, pp. 41-65.

Pais, M.A., Le Mouël, J.L., Lambeck, K., Poirier, J.P., 1999. Late Precambrian paradoxical glaciation and obliquity of the Earth—a discussion of dynamical constraints. Earth and Planetary Science Letters 174, 155-171.

Peltier, W.R., Liu, Y., Crowley, J.W., 2007. Snowball Earth prevention by dissolved organic carbon remineralization. Nature 450, 813-818.

Peltier, W.R., Tarasov, L., Vettoretti, G., Solheim, L.P., 2004. Climate dynamics in deep time: modeling the "snowball bifurcation" and assessing the plausibility of its occurrence. In: Jenkins, G.S., McMenamin, M.A.S., McKey, C.P., Sohl, L. (Eds.), The Extreme Proterozoic: Geology, Geochemistry, and Climate. Geophysical Monograph 146, American Geophysical Union, Washington, DC., pp. 107-124.

Perry, W.J., Roberts, H.G., 1968. Late Precambrian glaciated pavements in the Kimberley Region, Western Australia. Journal of the Geological Society of Australia 15(1), 51-56.

Pierrehumbert, R.T., 2004. High levels of atmospheric carbon dioxide necessary for the termination of global glaciation. Nature 429, 646-649.

Pisarevsky, S.A., Murphy, J.B., Cawood, P.A., Collins, A.S., 2008. Late Neoproterozoic and Early Cambrian palaeogeography: models and problems. In: Pankhurst, R.J., Trouw, R.A.J., Brito Neves, B.B., de Wit, M.J. (Eds.), West Gondwana: Pre-Cenozoic Correlations Across the South Atlantic Region. Geological Society, London, Special Publication 294, pp. 9-31.

Poidevin, J.-L., 2007. Stratigraphie isotopique de strontium et datation des formations carbonatées et glaciogéniques néoprotérozoiques du nord et de l'ouest du craton de Congo. C. R. Geoscience 339, 259-273.

Prave, A.R., 1999. Two diamictites, two cap carbonates, two $\delta^{13}C$ excursions, two rifts: The Neoproterozoic Kingston Peak Formation, Death Valley, California. Geology 27, 339-342.

Preiss, W.V., 1987. The Adelaide Geosyncline: Late Proterozoic stratigraphy, sedimentation, palaeontology and tectonics. Geological Survey of South Australia Bulletin 53, 438 p.

Rankin, D.W., 1993. The volcanogenic Mount Rogers Formation and the overlying glacigenic Konnarock Formation: two late Proterozoic units in southwestern Virginia. United States Geological Survey, Washington, DC.

Raub, T.D., Evans, D.A.D., 2006. Magnetic reversals in basal Ediacaran cap carbonates: a critical review. Eos, Transactions of the American Geophysical Union 87(36), Joint Assembly Supplement, Abstract GP41-02.

Ridgwell, A.J., Kennedy, M.J., Caldeira, K., 2003. Carbonate deposition, climate stability, and Neoproterozoic ice ages. Science 302, 859-862.

Rieu, R., Allen, P.A., Etienne, J.L., Cozzi, A., Wiechert, U., 2006. A Neoproterozoic glacially influenced basin margin succession and 'atypical' cap carbonate associated with bedrock paleovalleys, Mirbat area, southern Oman. Basin Research 18, 471-496.

Rieu, R., Allen, P.A., Cozzi, A., Kosler, J., Bussy, F., 2007. A composite stratigraphy for the Neoproterozoic Huqf Supergroup of Oman: initegrating new litho-, chemo- and chronostratigrapic data of the Mirbat area, southern Oman. Journal of the Geological Society, London 164, 997-1009.

Rocha-Campos, A.C., Hasui, Y., 1981. Tillites of the Macaúbas Group (Proterozoic) in central Minas Gerais and southern Bahia, Brazil. In: Hambrey, M.J., Harland, W.B. (Eds.), Earth's Pre-Pleistocene Glacial Record. Cambridge University Press, Cambridge, pp. 933-938.

Rodgers, J., 1957. The distribution of marine carbonate sediments: a review. In: Le Blanc, R.J., Breeding, J.G. (Eds.), Regional Aspects of Carbonate Deposition. Society of Economic Paleontologists and Mineralogists (SEPM), Special Publication 5, Tulsa, Oklahoma, pp. 2-14.

Sayles, R.W., 1914. The Squantum Tillite. Bulletin of the Museum of Comparative Zoology at Harvard College 56, 141-175, 12 plates, Cambridge, MA.

Schermerhorn, L.J.G., Stanton, W.I., 1963. Tilloids in the West Congo geosyncline. Quarterly Journal of the Geological Society of London 119, 201-241.

Schmidt, P.W., Williams, G.E., 1995. The Neoproterozoic climatic paradox: Equatorial paleolatitude for Marinoan glaciation near sea level in South Australia. Earth and Planetary Science Letters 134, 107-124.

Shields, G.A., 2005. Neoproterozoic cap carbonates: a critical appraisal of existing models and the plumeworld hypothesis. Terra Nova 17, 299-310.

Shields, G.A., Deynoux, M., Culver, S.J., Brasier, M.D., Affaton, P., Vandamme, D., 2007a. Neoproterozoic glaciomarine and dap dolostone facies of the southwestern Taoudéni Basin (Walidiala Valley, Senegal/Guinea, NW Africa). C. R. Geoscience 339, 186-199.

Shields, G.A., Deynoux, M., Strauss, H., Paquet, H., Nahon, D., 2007b. Barite-bearing cap dolostone of the Taoudéni Basin, northwest Africa: sedimentary and isotopic evidence for methane seepage after a Neoproterozoic glaciation. Precambrian Research 154, 209-235.

Sohl, L.E., Christie-Blick, N., Kent, D.V., 1999. Paleomagnetic polarity reversals in Marinoan (ca 600 Ma) glacial deposits of Australia: implications for the duration of low-latitude glaciation in Neoproterozoic time. Geological Society of America Bulletin 111, 1120-1139.

Sovetov, J., 2008. Marinoan glaciation in the Siberian craton: locality, erosional forms, deposits and conastraints to age. 33rd International Geological Congress, Abstracts, Session CGC-04.

Sovetov, Yu.K., Komlev, D.A. 2005. Tillites at the base of the Oselok Group, foothills of the Sayan Mountains, and the Vendian lower boundary in the southwestern Siberian Platform. Stratigraphy and Geological Correlations, 13, 337-366.

Spencer, A.M., 1971. Late Pre-Cambrian glaciation in Scotland. Geological Society of London Memoir 6, 99 pp.

Stern, R.J., Avigad, D., Miller, N.R., Beyth, M., 2006. Evidence for the Snowball Earth hypothesis in the Arabian-Nubian Shield and the East African Orogen. Journal of African Earth Sciences 44, 1-20.

Thompson, M.D., Bowring, S.A., 2000. Age of the Squantum “tillite”, Boston Basin, Massachusetts: U-Pb zircon constraints on terminal Neoproterozoic glaciation. American Journal of Science 300, 630-655.

Trindade, R.I.F., Macouin, M., 2007. Paleolatitude of glacial deposits and paleogeography of Neoproterozoic ice ages. C. R. Geoscience 339, 200-211.

Trompette, R., 1981. Late Precambrian tillites of the Volta Basin and the Dahomeyides Orogenic Belt (Benin, Ghana, Togo and Upper-Volta). In: Hambrey, M.J., Harland, W.B. (Eds.), Earth’s Pre-Pleistocene Glacial Record. Cambridge University Press, Cambridge, pp. 135-139.

Trompette, R., de Alvarenga, C.J.A., Wade, D., 1998. Geological evolution of the Neoproterozoic Corumbá graben system (Brazil). Depositional context of the stratified Fe and Mn ores of the Jacadigo Group. Journal of South American Earth Sciences 11, 587-597.

Walker, J.C.G., Hays, P.B., Kasting, J.F., 1981. A negative feedback mechanism for the long-term stabilization of Earth’s surface temperature. Journal of Geophysical Research 86(C10), 9776-9782.

Wang, J., Li, Z.-X., 2003. History of Neoproterozoic rift basins in South China: implications for Rodinia break-up. Precambrian Research 122, 141-158.

Wells, A.T., 1981. Late Proterozoic diamictites of the Amadeus and Ngalia Basins, central Australia. In: Hambrey, M.J., Harland, W.B. (Eds.), Earth’s Pre-Pleistocene Glacial Record. Cambridge University Press, Cambridge, pp. 515-524.

Whitten, G.F., 1970. The investigation and exploitation of the Razorback Ridge iron deposit. Geological Survey of South Australia Reports of Investigations 33, 165 p.

Williams, G.E., 1975. Late Precambrian glacial climate and the Earth's obliquity. Geological Magazine 112, 441-544.

Williams, G.E., 1986. Precambrian permafrost horizons as indicators of palaeoclimate. Precambrian Research 32, 233-242.

Williams, G.E., 1998. Late Neoproterozoic periglacial aeolian sand sheet, Stuart Shelf, South Australia. Australian Journal of Earth Sciences 45, 733-741.

Williams, G.E., 2000. Geological constraints on the Precambrian history of Earth's rotation and the Moon's orbit. Reviews of Geophysics 38(1), 37-59.

Williams, G.E., Schmidt, P.W., 2004. Neoproterozoic glaciation: reconciling low paleolatitudes and the geologic record. In: Jenkins, G.S., McMenamin, M.A.S., McKey, C.P., Sohl, L. (Eds*.),* The Extreme Proterozoic: Geology, Geochemistry, and Climate*.* Geophysical Monograph 146, American Geophysical Union, Washington, DC., pp. 145-159.

Williams, G.E., Tonkin, D.G., 1985. Periglacial structures and paleoclimatic significance of a late Precambrian block field in the Cattle Grid copper mine, Mount Gunson, South Australia. Australian Journal of Earth Sciences 32, 287-300.

Williams, G.E., Gostin, V.A., McKirdy, D.M., Preiss, W.V., 2008. The Elatina glaciation, late Cryogenian (Marinoan Epoch), South Australia: Sedimentary facies and palaeoenvironments. Precambrian Research 163, 307-331.

Worseley, T.R., Kidder, D.L., 1991. First-order coupling of paleogeography and CO_2, with global surface temperature and its latitudinal contrast. Geology 19, 1161-1164.

Xiao, S.-H., Bao, H.-M, Wang, H., Kaufman, A.J., Zhou, C., Li, G., Yuan, X., Ling, H., 2004. The Neoproterozoic Quruqtagh Group in eastern Chinese Tianshan: evidence for a post-Marinoan glaciation. Precambrian Research 130, 1-26.

Xu, B., Xiao, S., Zou, H.-B., Chen, Y., Li, Z.-X., Song, B., Liu, D.-Y., Zhou, C.-M., Yuan, X.-L., 2009. SHRIMP zircon U-Pb age constraints on Neoproterozoic Quruqtagh diamictites in NW China. Precambrian Research 168, 247-258.

Yin, C.-Y., Tang, F., Liu, Y.-Q., Gao, L.-Z., Liu, P.-J.Xing, Y.-S., Yang, Z.-Q., Wan, Y.-S., Wang, Z.-Q., 2005. U-Pb zircon age from the base of the Doushantuo Formation in the Yangtze Gorges, South China: constraint on the age of the Marinoan glaciation. Episodes 28, 48-49.

Young, G.M., 1976. Iron-formation and glaciogenic rocks of the Rapitan Group, Northwest Territories, Canada. Precambrian Research 3, 137-158.

Young, G.M., 2002. Stratigraphic and tectonic settings of Proterozoic glaciogenic rocks and banded iron-formations: relevance to the snowball Earth debate. Journal of African Earth Sciences 35, 451-466.

Zhang, Q.-R., Li, X.-H., Feng, L.-J., Huang, J., Biao, S., 2008. A new age constraint on the onset of the Neoproterozoic glaciations in the Yangtze Platform, South China. Journal of Geology 116, 423-429.

Zhang, S.-H., Jiang, G.-Q., Zhang, J.-M., Song, B., Kennedy, M.J., Christie-Blick, N., 2005. U-Pb sensitive high-reslution ion microprobe ages from the Doushantuo Formation in south China: constraints on late Neoproterozoic glaciations. Geology 33, 473-476.

Zhang, S.-H, Jiang, G., Han, Y., 2008. The age of the Nantuo Formation and Nantuo glaciation in South China. Terra Nova 20, 289-294.

Zhang, S.-H, Li, Z.-X., Wu, H., 2006. New Precambrian palaeomagnetic constraints on the position of the North China block in Rodinia. Precambrian Research 144, 213-238.

Zhou, C.-M., Tucker, R., Xiao, S.-H., 2004. New constraints on the age of Neoproterozoic glaciation in South China. Geology 32, 437-440.

Ziegler, A.M., Hulver, M.L., Lottes, A.L., Schmachtenberg, W.F., 1984. Uniformitarianism and paleoclimates: Inferences from the distribution of carbonate rocks. In: Brenchley, P.J. (Ed.), Fossils and Climate. John Wiley and Sons, New York, pp. 3-25.

Figure captions

Fig. 1. Present distribution of Ediacaran, Marinoan and Sturtian glacigenic formations (see Table 1). Raisz's 'armadillo' projection.

Fig. 2. U-Pb zircon radiometric age constraints on Ediacaran glaciation. Shaded area indicates the possible age range of glaciation.

Fig. 3. U-Pb zircon radiometric age constraints on Marinoan glaciation. Shaded area indicates the possible age range of glaciation. Symbology as in Fig. 2.

Fig. 4. U-Pb zircon radiometric age constraints on the Nantuo Formation and the Nantuo glaciation, plotted against (A) stratigraphic depth and (B) time. Note that the Nantuo Formation may only represent the final stages of the Nantuo glaciation.

Fig. 5. U-Pb zircon radiometric age constraints on Sturtian glaciation(s). *The 686±4 Ma age for the Scout Mountain Member (Fanning and Link, 2008) was previously reported as 709±5 Ma (Fanning and Link, 2004). Shaded area indicates possible age range of glaciation. Symbology as in Fig. 2.

Fig. 6. Palaeogeographic maps (Li et al., 2008) for (A) 580 Ma, (B) 635 Ma and (C) 715 Ma, showing the distribution of Ediacaran, Marinoan and Sturtian glacigenic formations (stars), respectively. Stars are colour-coded by pre-glacial sucession: blue for carbonate, green for mixed carbonate-siliciclastic, yellow for siliciclastic, and white for volcanic successions or where there is a major hiatus beneath the glacigenic formation. Stars with heavy black outlines contain polygonal sand-wedges and those outlined in red contain sedimentary Fe or Fe-Mn deposits. For abbreviations of palaeocontinents see Table 1.

Fig. 7. Palaeomeridional distribution of (A) Ediacaran, (B) Marinoan and (C) Sturtian glacigenic formations based on palaeogeographic reconstructions (Fig. 6). See Table 1 for abbreviations of formation names and present locations. Grey lines indicate a random distribution. Note bias in favour of high palaeolatitudes in (A), and low palaeolatitudes in (B) and (C).

Fig. 8. Thickness of syn-deglacial Marinoan cap dolostones as a function of palaeolatitude. Note decrease in maximum thickness withn increasing palaeolatitude. The linked open and closed circles refer to Australian poles from the Elatina Formation (open circles) used by Li et al. (2008) to construct Fig. 6B and poles from the Nuccaleena Formation cap dolostone from Raub and Evans (2007), which imply that the Elatina poles have experienced a degree of inclination flattening due to compaction. Accordingly, palaeo-latitudes based on the Elatina poles (open circles) may be too low by ~8 degrees.

Fig. 9. Giant wave ripple in Marinoan cap dolostone (Nuccaleena Formation) near Elatina Creek (31°21.474´S, 138°37.054´E), central Flinders Ranges, South Australia. Note underformed strata above and below the wave ripple (a and b, correlative layers), and absence of a fault or void-filling cement. Linear ripple crests (n=23) in the vicinity have a mean azimuth of 009.22°, which was close to true north at 635 Ma (Fig. 6B). Hammer is 32.5 cm long.

Fig. 10. Azimuthal orientations of the crests of giant wave ripples (red bars) in Marinoan cap dolostones (see Table 2). Rose diagrams for individual directions (left) and regional mean directions (right) exclude data from Tuva-Mongolia (orange bars), for which no independent palaeomagnetic data are available. Note near-meridional (N-S) mean directions and lack of zonal (W-E) directions, consistent with formation of giant wave ripples by zonal wind-driven waves (Allen and Hoffman, 2005).

Fig. 11. Palaeogeographic map for 635 Ma (Li et al., 2008) showing colour-coded distribution of post-glacial cap-carbonate sequences.

Fig. 12. Distribution of (A) Marinoan and (B) Sturtian glacigenic deposits on palaeogeographic maps for 635 and 715 Ma (Li et al., 2008).

Table 1. Neoproterozoic glacigenic formations

Ediacaran (590-570 Ma)

Paleocontinent	*Sym.*	*Formation*	*Sym.*	*Succession/Basin*	*Reference*
Amazonia	Am	Serra Azul	Az	Alto Paraguay	Alvarenga et al. (2007)
Australia	Au	Egan	Eg	Kimberleys	Corkeron and George (2001)
Avalonia	Av	Gaskiers	Ga	Conception	Eyles and Eyles (1989)
		Squantum	Sq	Boston Bay	Sayles (1914)
Baltica	Ba	Mortensnes	Mt	Verstertana	Edwards (1984)
		Moelv	Mo	Sparagmite	Nystuen (1976)
		Vilchitsy	Vi	Eastern Europe	Chumakov (2004)
		Churochnaya	Cn	Urals	Chumakov (2004)
Cadomia	Ca	Granville	Gr	Brittany	Graindor (1964)
Laurentia	Laur	Loch na Cille	Lo	Dalradian	McCay et al. (2006)
North China	NC	Luoquan	Lq	Qinling	Guan et al. (1986)
Tarim	Tm	Hankalchough	Ha	Quruqtagh	Xiao et al. (2004)
[1]Tasmania	Ta	Croles Hill	Cr	Kanunnah	Calver et al. (2004)

Marinoan (655-635 Ma)

Amazonia	Am	Puga	Pu	Alto Paraguay	Alvarenga and Trompette (1992)
Arabia	Ar	Fiq	Fi	Huqf	Allen et al. (2004)
		Shareef	Sh	Mirbat	Rieu et al. (2007)
Australia	Au	Elatina	El	Adelaidean	Williams et al. (2008)
		Olympic	Ol	Amadeus	Wells (1981)
		Landrigan	La	Kimberleys	Coats and Preiss (1980)
Baltica	Ba	Smalfjord	Sm	Verstertana	Edwards (1984)
Congo	Co	Petite	Pe	Katangan	Cahen and Lepersonne (1981)
		Ghaub	Gh	Otavi	Hoffman and Halverson (2008)
		Supérieure	Sp	West Congolian	Schermerhorn and Stanton (1963)
		Bondo	Bo	Fouroumbala	Poidevin (2007)
Laurentia	Laur	Wildrose	Wr	Death Valley	Prave (1999)
		Vreeland	Vr	Rocky Mtns	McMechan (2000)
		Ice Brook (Stelfox)	Ib	Mackenzie Mtns	Aitken (1991)
		Storeelv	St	East Greenland	Hambrey and Spencer (1987)
		Wilsonbreen	Wb	East Svalbard	Harland et al. (1993)
		Stralinchy-Reelan	Re	Dalradian	McCay et al. (2006)
India	In	Blaini	Bl	Lesser Himalaya	Holland (1908)
Iran	Ir	Rizu	Ri	Lut	Hamdi (1992)
Kalahari	Ka	Numees	Nu	Gariep	Frimmel et al. (2002)
		Blässkranz	Bk	Witvlei	Miller (2008)
São Francisco	SF	Palestina	Pa	Bambuí	Misi et al. (2008)
Siberia	Si	Dzemkukan	Dz	Patom	Sovetov (2008)
		Marnya	Ma	Sayan	Sovetov and Komlev (2005)
		Pod'em	Pd	Yenisey	Sovetov (2008)
South China	SC	Nantuo	Na	Yangtze	Wang and Li (2003)
Tarim	Tm	Tereeken	Te	Quruqtagh	Xiao et al. (2004)
[1]Tasmania	Ta	Cottons	Co	King Island	Calver and Walter (2000)

Tuva-Mongolia	TM	Khongoryn	Kg	Dzabkhan	Macdonald et al. (2009a)
West Africa	WA	Jbéliat	Jb	Taoudéni (Adrar)	Deynoux (1985)
		Bakoye	Ba	Taoudéni (Mali)	Deynoux et al. (1991)
		Kodjari	Ko	Volta	Trompette (1981)
Sturtian (726-660 Ma)					
Akaska-Chukot	AC	Hula Hula	Hu	Sadlerochit	Macdonald et al. (2009b)
Arabia	Ar	Gubrah	Gu	Huqf	Le Guerroué et al. (2005)
		Ayn	Ay	Mirbat	Rieu et al. (2006)
		Tambien	Ta	Nubia	Stern et al. (2006)
Arequipa	Aq	Chiquerío	Cq	Chiquerío-Antafalla	Chew et al. (2007)
Australia	Au	Sturt	St	Adelaidean	Preiss (1987)
		Areyonga	Ar	Amadeus	Wells (1981)
Baltica	Ba	Tany	Ty	Urals	Chumakov (2004)
Congo	Co	[2]Grand	Gr	Katangan	Cahen and Lepersonne (1981)
		Chuos	Ch	Otavi	Hoffman and Halverson (2008)
		Inférieure	In	West Congolian	Schermerhorn and Stanton (1963)
		Akwokwo	Ak	Lindian	Poidevin (2007)
Laurentia	Laur	Surprise	Su	Death Valley	Prave (1999)
		Pocatello	Po	Idaho	Link (1983)
		Toby	To	Windermere	Aalto (1981)
		Rapitan	Ra	Mackenzie Mtns	Young (1976)
		Tindir	Ti	Tindir	Allison et al. (1981)
		Ulvesø	Ul	East Greenland	Hambrey and Spencer (1987)
		Petrovbreen	Pb	East Svalbard	Harland et al. (1993)
		Port Askaig	Pt	Dalradian	Spencer (1971)
		Konnarock	Kn	Blue Ridge	Miller (1994)
Kalahari	Ka	[2]Kaigas	Ka	Gariep	Frimmel et al. (2002)
		Blaubekker	Bb	Witvlei	Miller (2008)
Kazakhstan	Kz	Baykonur	Br	Kazakh	Chumakov (1978)
São Francisco	SF	Jequitaí	Je	Bambuí	Rocha-Campos and Hasui (1981)
Siberia	Si	Kharlukhtakh	Kh	Patom	Sovetov (2008)
		Chivida	Cv	Yenisey	Sovetov (2008)
South China	SC	Jiangkou	Ji	Yangtze	Wang and Li (2003)
Tarim	Tm	[2]Bayisi	By	Quruqtagh	Xiao et al. (2004)
[1]Tasmania	Ta	Julius River	Ju	Kanunnah	Calver (1998)
Tuva-Mongolia	TM	Maikhan Ul	Mk	Dzabkhan	Lindsay et al. (1996)

[1]Possibly part of the Australian rifted margin
[2]Possibly pre-Sturtian (i.e., pre-726 Ma)

Table 2. Azimuthal orientations of giant wave ripple crests in Marinoan cap dolostones

Palaeocontinent	Location	Name	Area	Azimuths
Amazonia	SW Brazil	Mirassol	Mirassol d'Oeste	170°
Arctic Alaska	NE Alaska	Nularvik	[1]Sadlerochit Mtns	172°, 175°
Australia	South Australia	Nuccaleena	[1]Brachina Gorge	005-015° (n=6; average 010°)
			Elatina Creek	000-015° (n=16; average 006.7°)
				013-018° (n=7; average 015°)
	Kimberleys, WA	Landrigan	Louisa Downs	030±10°
Congo	NC Namibia	Keilberg	Otavi Mountains	075°, 170°
	NW Namibia	Keilberg	Kaokoveld	110°, 119°, 126°, 133°, 140°
	NW Namibia	Keilberg	Fransfontein slope	085°, 092°, 100°, 118°, 120°
Kalahari	SW Namibia	Bloeddrif	[1]Namaskluft	092-115° (n=9; average 101.2°)
				107-120° (n=6; average 105.7°)
				97°
Laurentia	NW Canada	Ravensthroat	Arctic Red River	048°, 052°, 057°
			Cranswick River	005°
			Stoneknife River	010°
			Twitya River	030-050° (n=5; average 040°)
			Shale Lake	010-030° (n=4; average 22.5°)
			Stelfox Mountain	015°, 020°, 095°, 097°, 100°
			Ravensthroat River	075°
	East Svalbard	Dracoisen	Svaenor	085°
Tasmania	King Island	Cumberland Ck	Yarra Creek	000-015° (n=3; average 007°)
Tuva-Mongolia	SW Mongolia	Ol	[1]Dzabkhan	59°, 65°, 100°, 100°

[1]Data courtesy of Francis A. Macdonald (unpublished)

Ediacaran
583-581 Ma

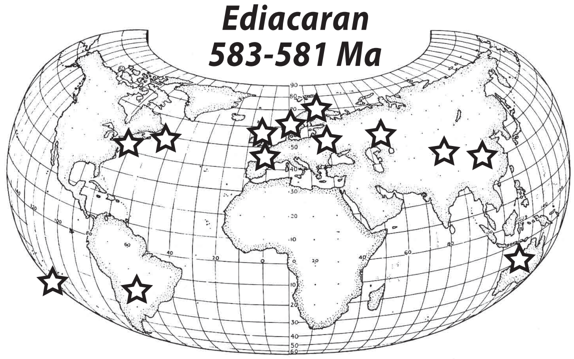

Marinoan
655-635 Ma

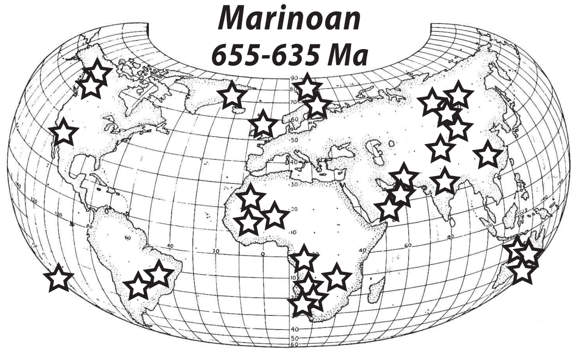

Sturtian
755-660 Ma

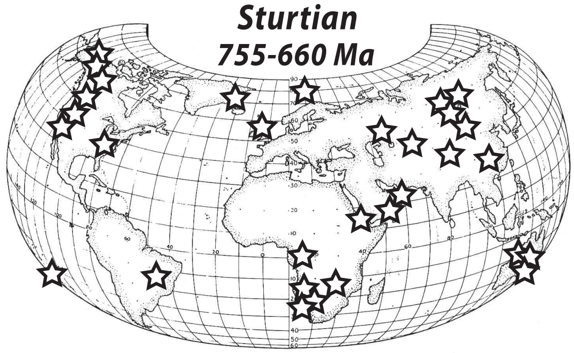

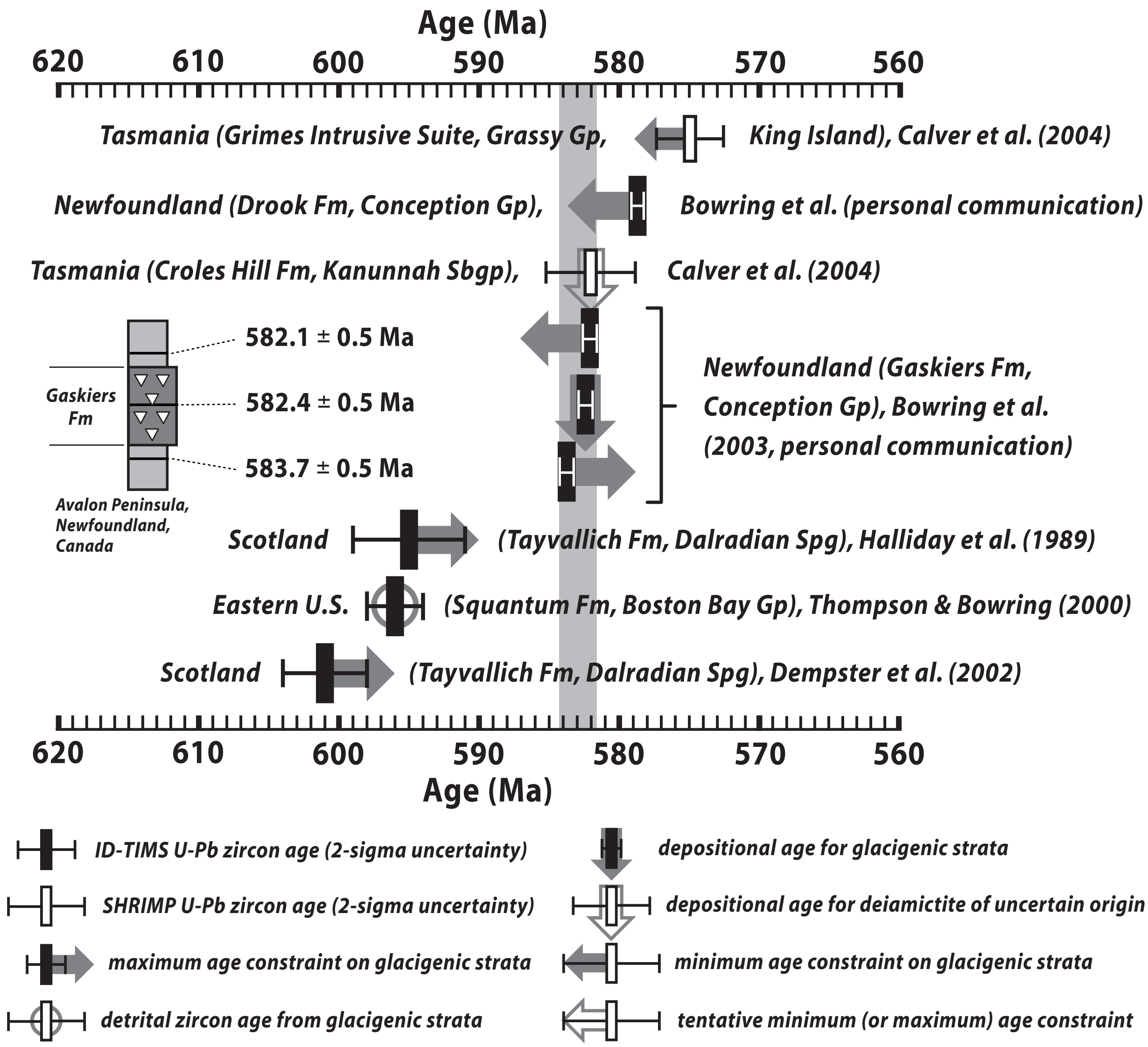
Age (Ma)
620
610
600
590
580
570
560
Tasmania (Grimes Intrusive Suite, Grassy Gp, King Island), Calver et al. (2004)
Newfoundland (Drook Fm, Conception Gp), Bowring et al. (personal communication)
Tasmania (Croles Hill Fm, Kanunnah Sbgp), Calver et al. (2004)
582.1 ± 0.5 Ma
Gaskiers Fm
582.4 ± 0.5 Ma
583.7 ± 0.5 Ma
Avalon Peninsula, Newfoundland, Canada
Newfoundland (Gaskiers Fm, Conception Gp), Bowring et al. (2003, personal communication)
Scotland (Tayvallich Fm, Dalradian Spg), Halliday et al. (1989)
Eastern U.S. (Squantum Fm, Boston Bay Gp), Thompson & Bowring (2000)
Scotland (Tayvallich Fm, Dalradian Spg), Dempster et al. (2002)
620
610
600
590
580
570
560
Age (Ma)
ID-TIMS U-Pb zircon age (2-sigma uncertainty)
SHRIMP U-Pb zircon age (2-sigma uncertainty)
maximum age constraint on glacigenic strata
detrital zircon age from glacigenic strata
depositional age for glacigenic strata
depositional age for deiamictite of uncertain origin
minimum age constraint on glacigenic strata
tentative minimum (or maximum) age constraint

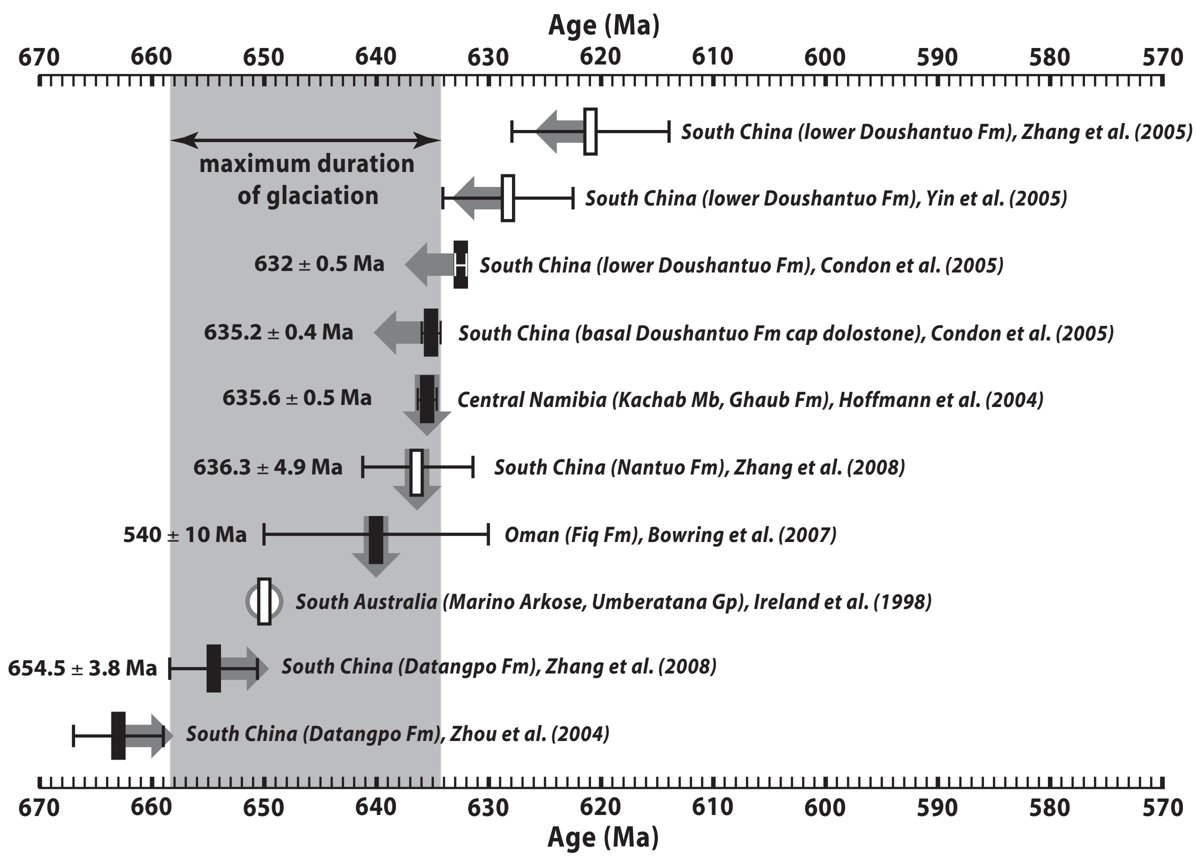
Age (Ma)
670
660
650
640
630
620
610
600
590
580
570
maximum duration
of glaciation
South China (lower Doushantuo Fm), Zhang et al. (2005)
South China (lower Doushantuo Fm), Yin et al. (2005)
632 ± 0.5 Ma
South China (lower Doushantuo Fm), Condon et al. (2005)
635.2 ± 0.4 Ma
South China (basal Doushantuo Fm cap dolostone), Condon et al. (2005)
635.6 ± 0.5 Ma
Central Namibia (Kachab Mb, Ghaub Fm), Hoffmann et al. (2004)
636.3 ± 4.9 Ma
South China (Nantuo Fm), Zhang et al. (2008)
540 ± 10 Ma
Oman (Fiq Fm), Bowring et al. (2007)
South Australia (Marino Arkose, Umberatana Gp), Ireland et al. (1998)
654.5 ± 3.8 Ma
South China (Datangpo Fm), Zhang et al. (2008)
South China (Datangpo Fm), Zhou et al. (2004)
Age (Ma)

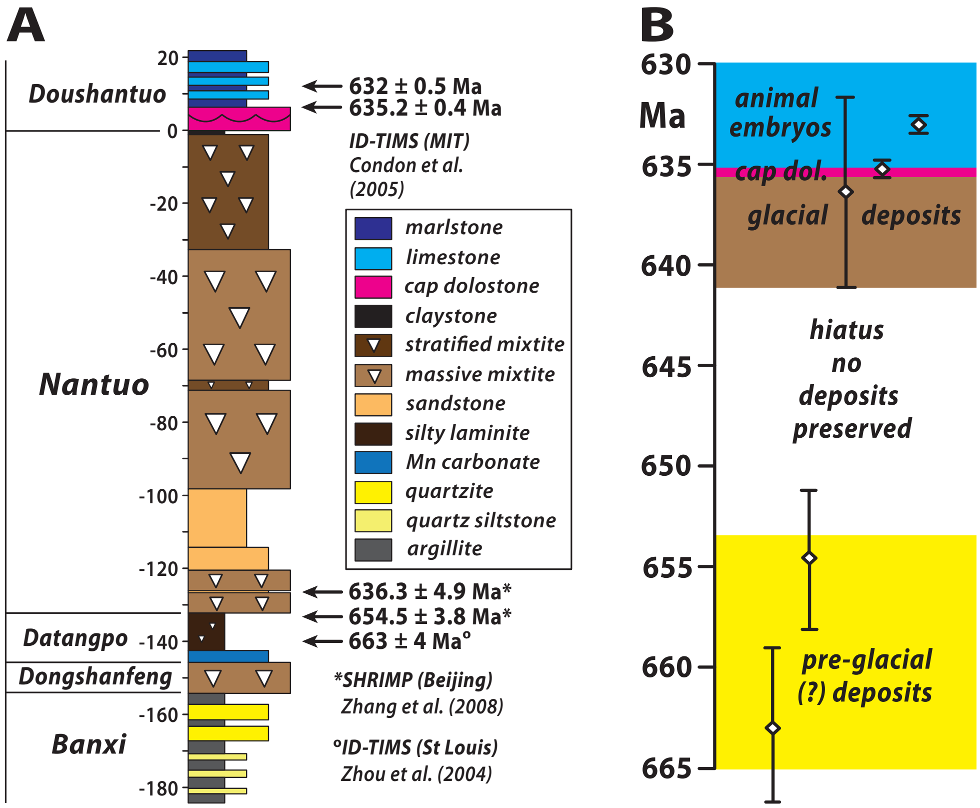

A
Doushantuo
Nantuo
Datangpo
Dongshanfeng
Banxi
20
0
-20
-40
-60
-80
-100
-120
-140
-160
-180
632 ± 0.5 Ma
635.2 ± 0.4 Ma
ID-TIMS (MIT)
Condon et al.
(2005)
marlstone
limestone
cap dolostone
claystone
stratified mixtite
massive mixtite
sandstone
silty laminite
Mn carbonate
quartzite
quartz siltstone
argillite
636.3 ± 4.9 Ma*
654.5 ± 3.8 Ma*
663 ± 4 Ma°
*SHRIMP (Beijing)
Zhang et al. (2008)
°ID-TIMS (St Louis)
Zhou et al. (2004)
B
Ma
630
635
640
645
650
655
660
665
animal
embryos
cap dol.
glacial
deposits
hiatus
no
deposits
preserved
pre-glacial
(?) deposits

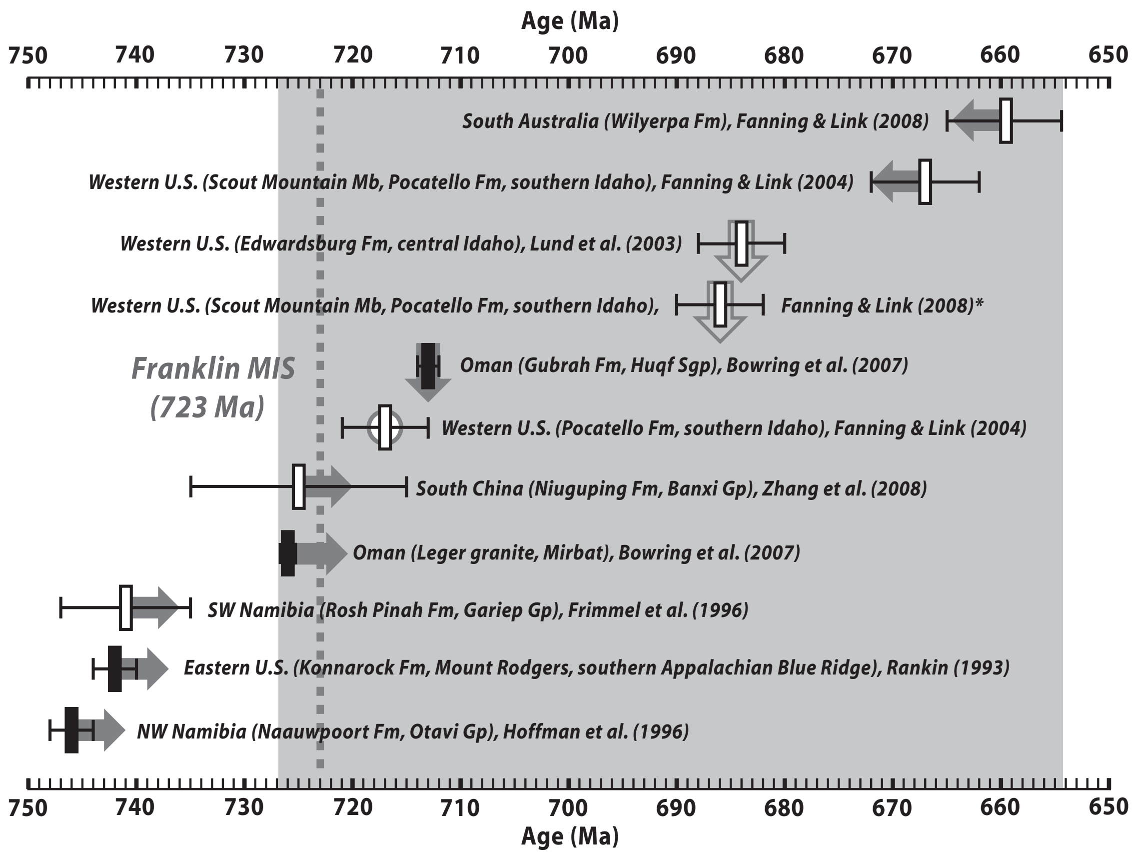

Age (Ma)
750
740
730
720
710
700
690
680
670
660
650
South Australia (Wilyerpa Fm), Fanning & Link (2008)
Western U.S. (Scout Mountain Mb, Pocatello Fm, southern Idaho), Fanning & Link (2004)
Western U.S. (Edwardsburg Fm, central Idaho), Lund et al. (2003)
Western U.S. (Scout Mountain Mb, Pocatello Fm, southern Idaho),
Fanning & Link (2008)*
Franklin MIS
(723 Ma)
Oman (Gubrah Fm, Huqf Sgp), Bowring et al. (2007)
Western U.S. (Pocatello Fm, southern Idaho), Fanning & Link (2004)
South China (Niuguping Fm, Banxi Gp), Zhang et al. (2008)
Oman (Leger granite, Mirbat), Bowring et al. (2007)
SW Namibia (Rosh Pinah Fm, Gariep Gp), Frimmel et al. (1996)
Eastern U.S. (Konnarock Fm, Mount Rodgers, southern Appalachian Blue Ridge), Rankin (1993)
NW Namibia (Naauwpoort Fm, Otavi Gp), Hoffman et al. (1996)

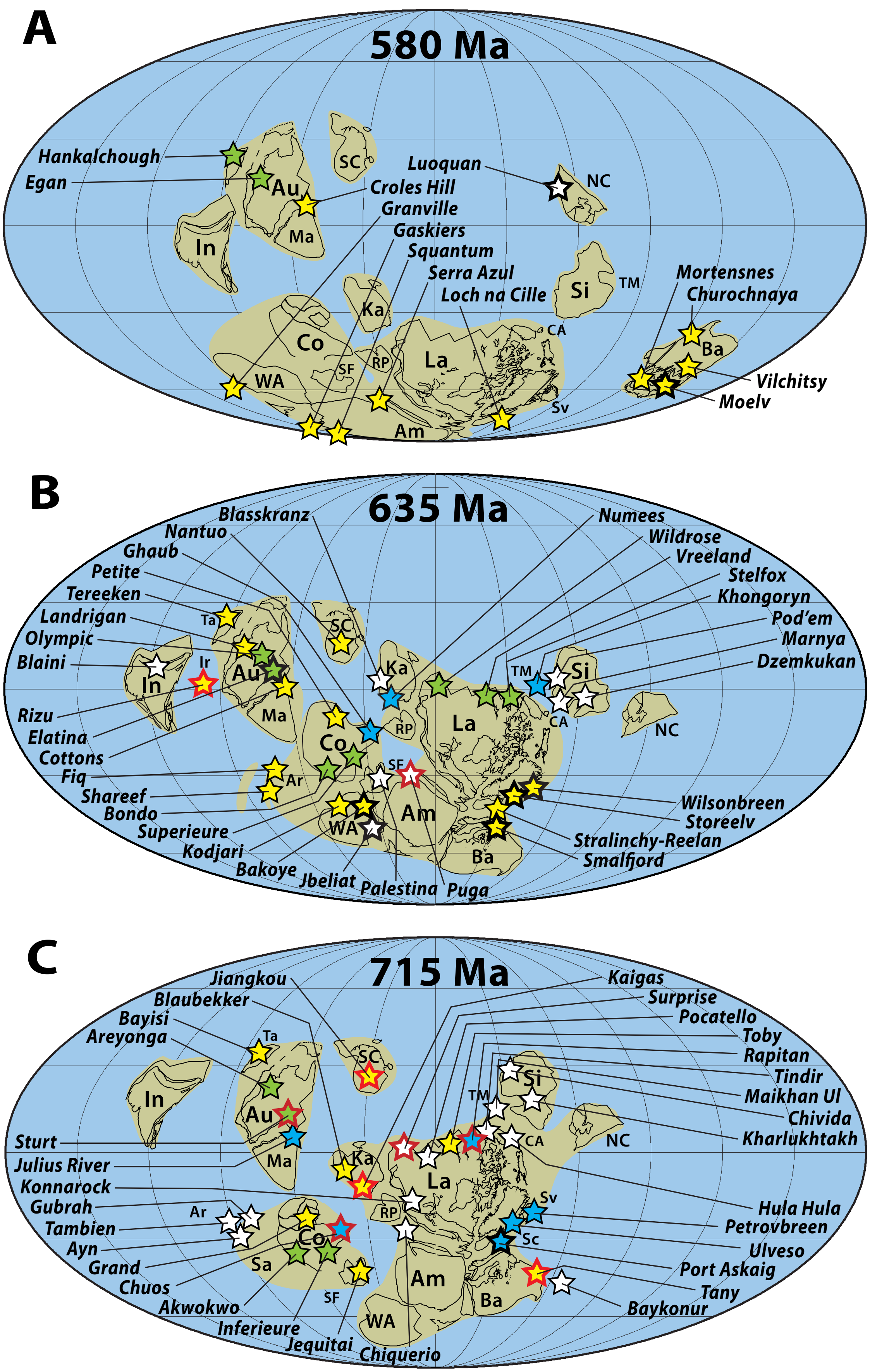
A
580 Ma
Hankalchough
Egan
Au
SC
In
Ma
Croles Hill
Granville
Gaskiers
Squantum
Serra Azul
Loch na Cille
Luoquan
NC
Si
TM
Ka
Co
SF
RP
La
CA
WA
Am
Sv
Mortensnes
Churochnaya
Ba
Vilchitsy
Moelv
B
635 Ma
Blasskranz
Nantuo
Ghaub
Petite
Tereeken
Landrigan
Olympic
Blaini
Rizu
Elatina
Cottons
Fiq
Shareef
Bondo
Superieure
Kodjari
Bakoye
Jbeliat
Palestina
Puga
Numees
Wildrose
Vreeland
Stelfox
Khongoryn
Pod'em
Marnya
Dzemkukan
Wilsonbreen
Storeelv
Stralinchy-Reelan
Smalfjord
Ta
Ir
In
Au
Ma
SC
Ka
RP
Co
Ar
SF
WA
Am
Ba
La
TM
Si
CA
NC
C
715 Ma
Jiangkou
Blaubekker
Bayisi
Areyonga
Sturt
Julius River
Konnarock
Gubrah
Tambien
Ayn
Grand
Chuos
Akwokwo
Inferieure
Jequitai
Chiquerio
Kaigas
Surprise
Pocatello
Toby
Rapitan
Tindir
Maikhan Ul
Chivida
Kharlukhtakh
Hula Hula
Petrovbreen
Ulveso
Port Askaig
Tany
Baykonur
Ta
In
Au
Ma
SC
Ka
RP
Ar
Co
Sa
SF
WA
Am
La
TM
Si
CA
NC
Sv
Sc
Ba

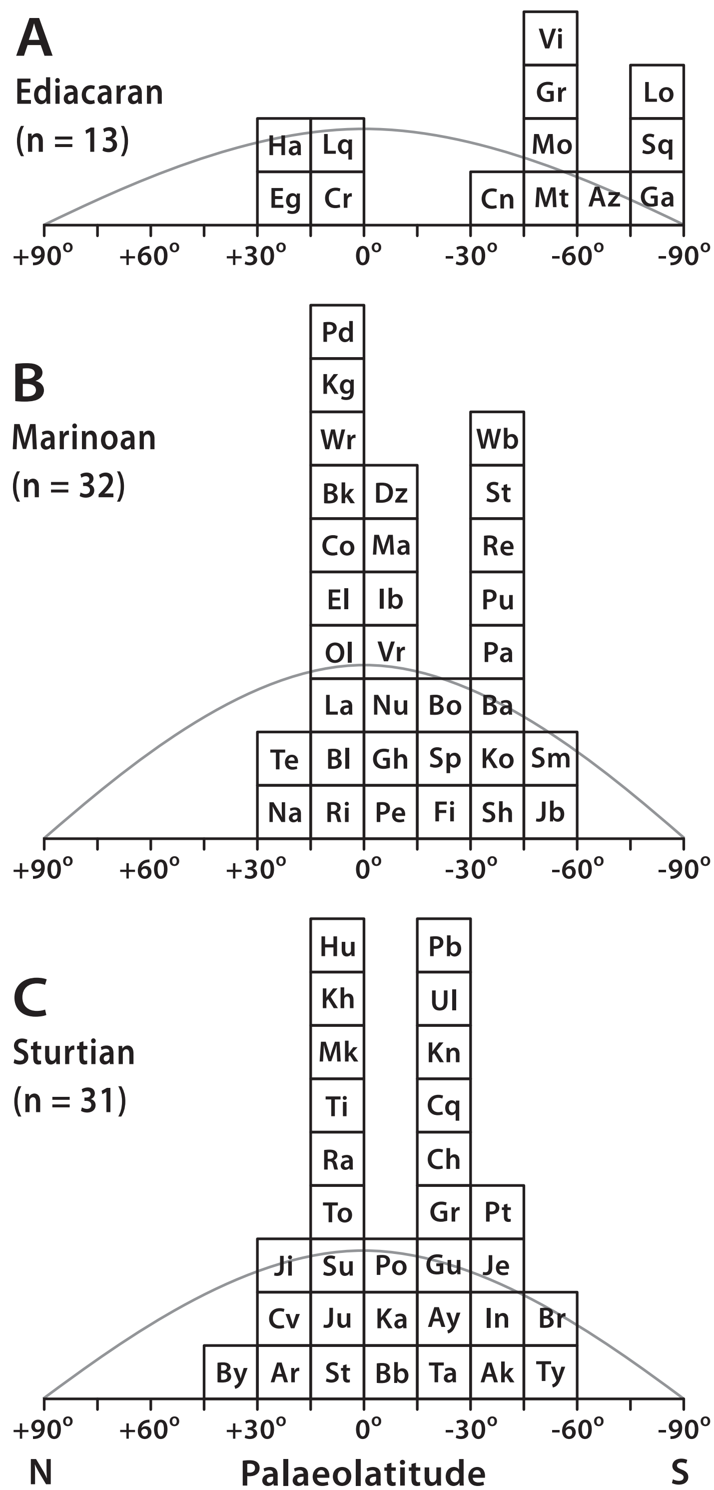
A
Ediacaran
(n = 13)
Vi
Gr
Lo
Ha
Lq
Mo
Sq
Eg
Cr
Cn
Mt
Az
Ga
+90º
+60º
+30º
0º
-30º
-60º
-90º
B
Marinoan
(n = 32)
Pd
Kg
Wr
Wb
Bk
Dz
St
Co
Ma
Re
El
Ib
Pu
Ol
Vr
Pa
La
Nu
Bo
Ba
Te
Bl
Gh
Sp
Ko
Sm
Na
Ri
Pe
Fi
Sh
Jb
+90º
+60º
+30º
0º
-30º
-60º
-90º
C
Sturtian
(n = 31)
Hu
Pb
Kh
Ul
Mk
Kn
Ti
Cq
Ra
Ch
To
Gr
Pt
Ji
Su
Po
Gu
Je
Cv
Ju
Ka
Ay
In
Br
By
Ar
St
Bb
Ta
Ak
Ty
+90º
+60º
+30º
0º
-30º
-60º
-90º
N
Palaeolatitude
S

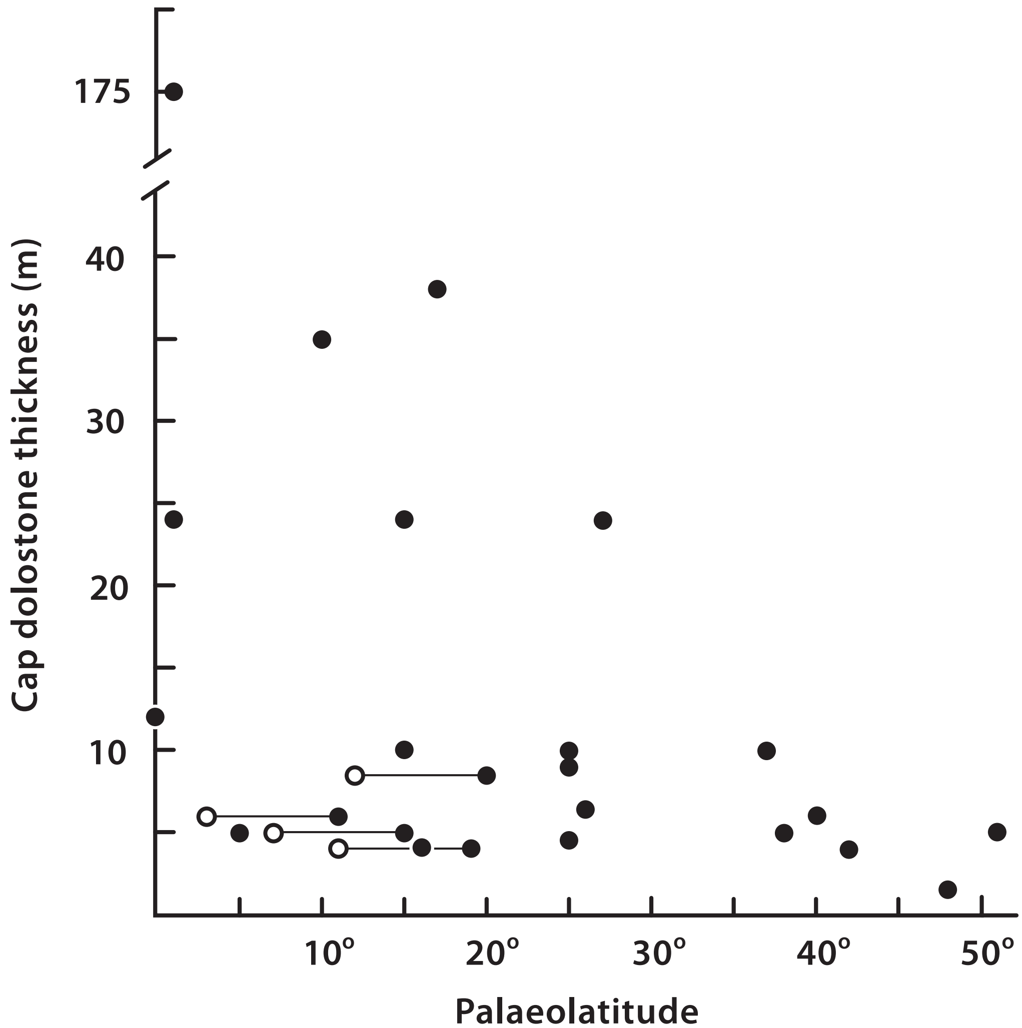
175
40
30
20
10
Cap dolostone thickness (m)
10°
20°
30°
40°
50°
Palaeolatitude


a
b
a
b

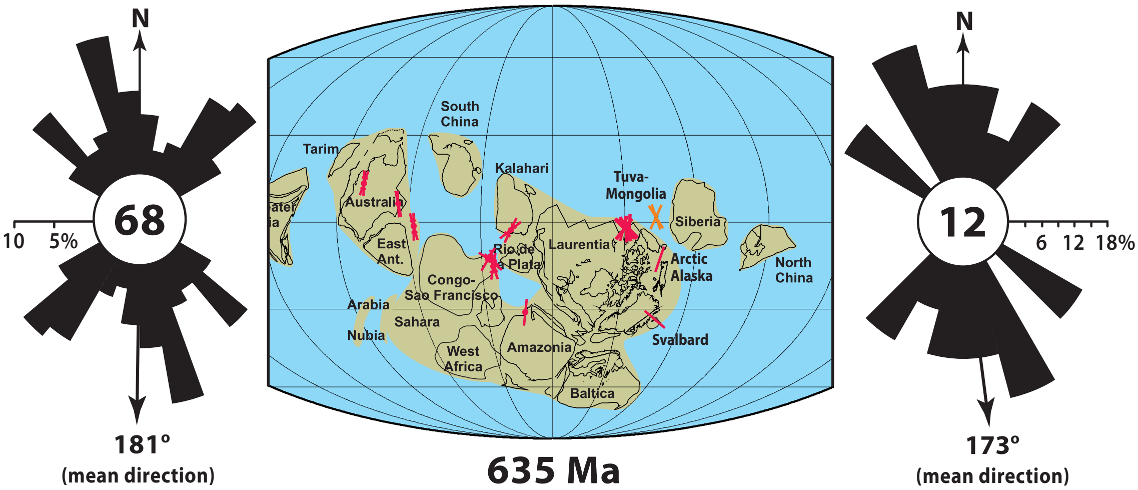
N
68
10
5%
181°
(mean direction)
South China
Tarim
Australia
East Ant.
Kalahari
Tuva-
Mongolia
Siberia
Laurentia
Rio de
a Plata
Arctic
Alaska
North
China
Congo-
Sao Francisco
Arabia
Sahara
Nubia
West
Africa
Amazonia
Svalbard
Baltica
635 Ma
N
12
6
12
18%
173°
(mean direction)

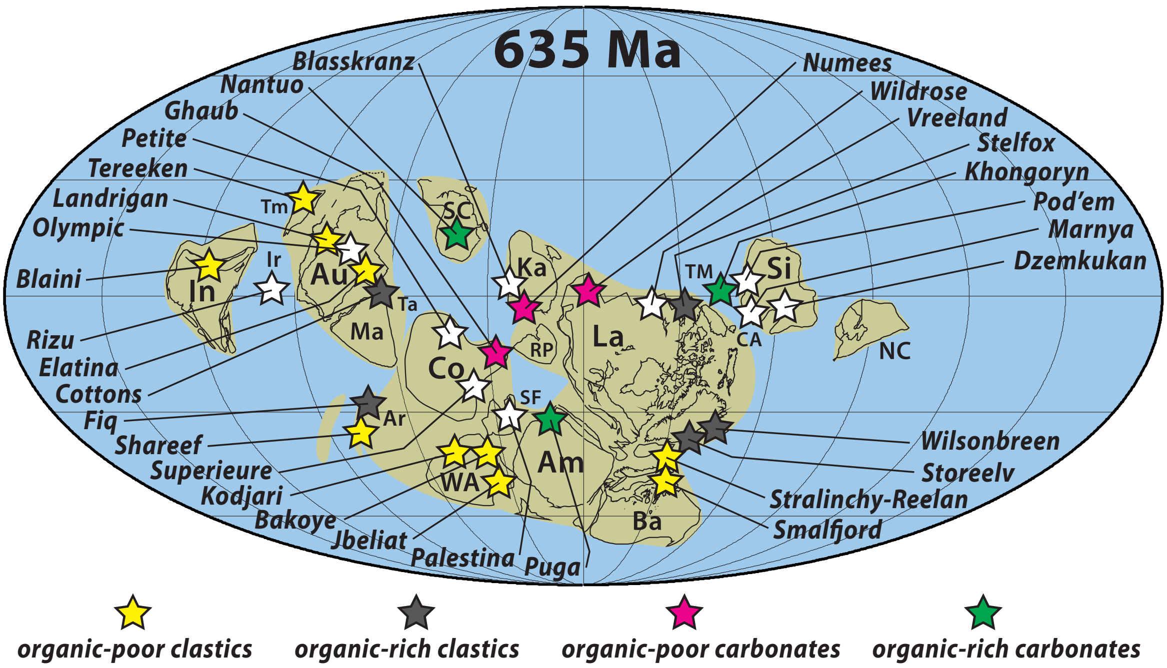
635 Ma
Blasskranz
Nantuo
Ghaub
Petite
Tereeken
Landrigan
Olympic
Blaini
Rizu
Elatina
Cottons
Fiq
Shareef
Superieure
Kodjari
Bakoye
Jbeliat
Palestina
Puga
Numees
Wildrose
Vreeland
Stelfox
Khongoryn
Pod'em
Marnya
Dzemkukan
Wilsonbreen
Storeelv
Stralinchy-Reelan
Smalfjord
Tm
Ir
In
Au
Ta
Ma
SC
Ka
RP
Co
Ar
SF
WA
Am
La
TM
Si
CA
NC
Ba
organic-poor clastics
organic-rich clastics
organic-poor carbonates
organic-rich carbonates

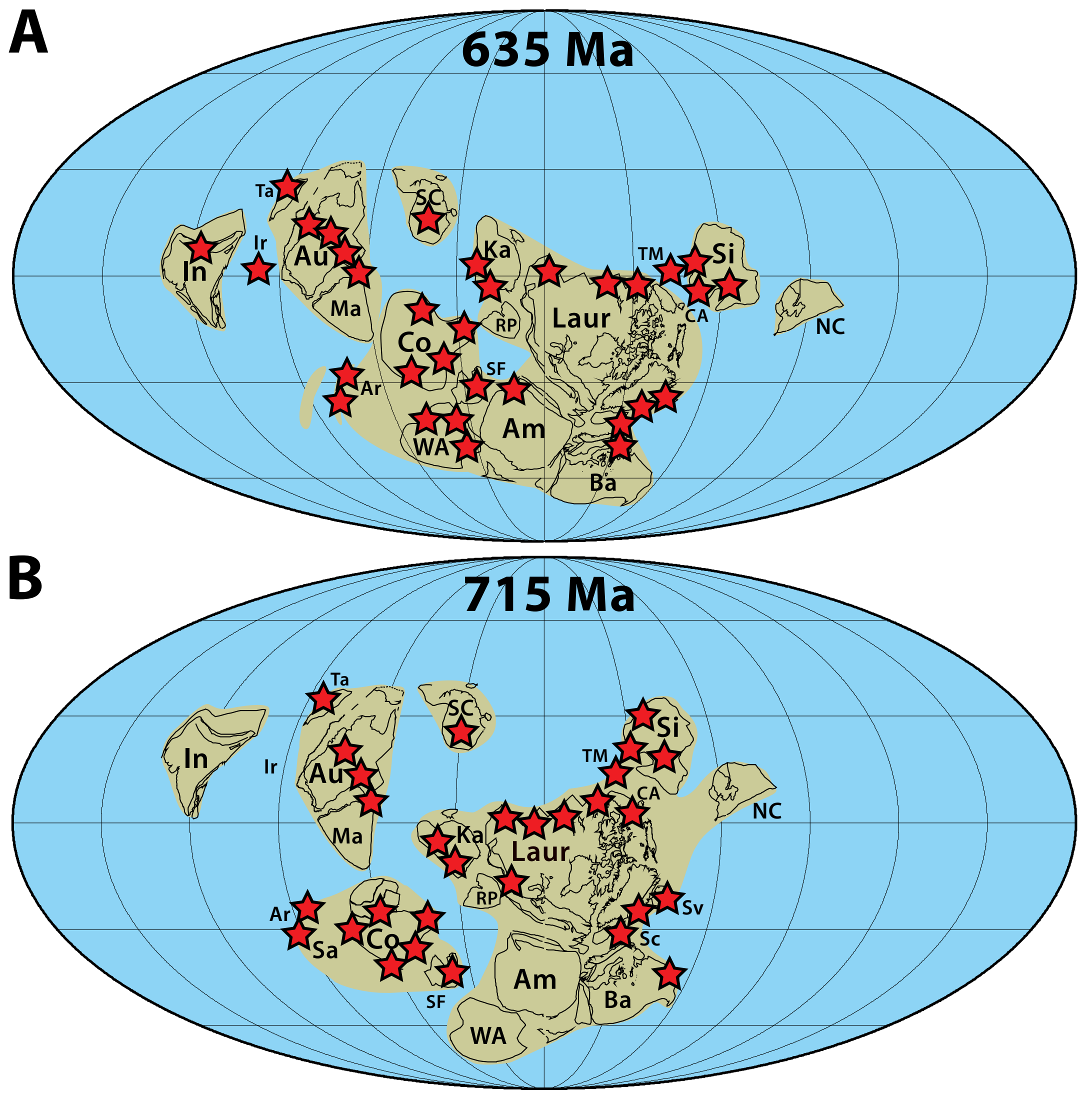
A
635 Ma
Ta
SC
Ir
In
Au
Ka
TM
Si
Ma
RP
Laur
CA
NC
Co
SF
Ar
Am
WA
Ba
B
715 Ma
Ta
SC
Si
In
Ir
Au
TM
CA
NC
Ka
Ma
Laur
RP
Sv
Ar
Sa
Co
Sc
Am
SF
Ba
WA